GL-TR-90-0109

JOURNAL OF GEOPHYSICAL RESEARCH, VOL. 94, NO. A12, PAGES 16,925–16,944, DECEMBER 1, 1989

Thermospheric Dynamics During September 18–19, 1984
1. Model Simulations

G. CROWLEY,[1] B. A. EMERY, AND R. G. ROBLE

High Altitude Observatory, National Center for Atmospheric Research, Boulder, Colorado

H. C. CARLSON, JR.

Air Force Geophysics Laboratory, Hanscom Air Force Base, Bedford, Massachusetts

D. J. KNIPP

Physics Department, U.S. Air Force Academy, Colorado Springs, Colorado

For realistic predictions of global thermospheric dynamics using thermospheric general circulation models (TGCMs), one of the main problems lies in the specification of the three-dimensional, time-dependent forcing fields for any given day. The September 18–19, 1984, Equinox Transition Study (ETS) interval was simulated using the National Center for Atmospheric Research TGCM with inputs guided by observations. During the ETS campaign, large quantities of high-quality data were available from high latitudes, and the high-latitude forcings for the TGCM could therefore be defined with precision for this period. The importance of upward propagating semidiurnal tides is also emphasized. This is the first realistic time-dependent simulation to incorporate upward propagating tides. Magnetically quiet conditions prevailed for several days prior to the magnetic storm which began about 0930 UT on September 19, 1984. The storm generated major disturbances in the global circulation, temperature, and composition of the thermosphere. A description of the simulated quiet time thermospheric structure for September 18 is contrasted with the storm time behavior on September 19. Several features of the storm response are described, including the generation of large-scale equatorward propagating disturbances. Longer-lived perturbations of the neutral temperature and composition are also discussed. A new feature has been discovered in the model predictions for altitudes around 200 km. This feature comprises a quasi-fixed four-cell pattern of high- and low-density regions in the polar cap. The exact location of the feature varies with UT, and the magnitude of the density perturbations depends on the strength of the high-latitude convection.

1. INTRODUCTION

The experimental phase of the Equinox Transition Study (ETS) took place between September 17 and 24, 1984. One of the initial objectives of the ETS was to investigate changes in the thermospheric circulation at the transition from one zonal mean solstice pattern (June) to another (December). These changes are predicted to occur within a week of equinox and have important implications for seasonal variations of temperature, density, and composition in the thermosphere [*Roble et al.*, 1977]. The broader aim of ETS is to understand the electromechanical response of the ionosphere-thermosphere system to variable high-latitude forcing [*Carlson and Crowley*, this issue].

The experimental design resulted in a large quantity of high-quality data, and coverage was global rather than mesoscale. Eight polar-orbiting satellites, five incoherent scatter radars, and many other diagnostics measured neutral and charged particle densities, temperatures, winds, electric fields, and energetic particle precipitation. The 8-day period involved the most disturbed day of the year and a day half as disturbed, separated and preceded by quiet days. The ETS data set was unique among campaigns of this nature and aroused a great deal of interest in the aeronomy community.

The development of the National Center for Atmospheric Research (NCAR) thermospheric general circulation model (TGCM) has been described in a series of papers by *Dickinson et al.* [1981, 1984], *Roble et al.* [1982, 1983], and *Fesen et al.* [1986]. *Roble et al.* [1987] and *Roble and Ridley* [1987] have described various parameterizations of high-latitude magnetospheric convection and auroral particle precipitation that have been incorporated in the NCAR TGCM. A diagnostic package for the TGCM has also been designed to analyze some of the physical processes that are operating within the model [*Killeen and Roble*, 1984].

In recent years, TGCMs have been developed to study the basic global circulation, temperature, and compositional structure of the thermosphere and its response to solar and auroral activity. The TGCMs have been used to examine the mean or averaged solar-driven thermospheric circulation for equinox and solstice conditions [*Fuller-Rowell and Rees*, 1980, 1983; *Dickinson et al.*, 1981, 1984], the response to auroral particle precipitation and model substorms [*Fuller-Rowell and Rees* 1981, 1984; *Smith et al.*, 1982; *Rees*, 1985; *Roble et al.*, 1987], the mean high-latitude thermospheric circulation in comparison with Dynamics Explorer satellite data [*Roble et al.*, 1983, 1984; *Rees et al.*, 1983, 1985, 1986; *Hays et al.*, 1984; *Killeen and Roble*, 1984], and the winds over a given ground station [*Hernandez and Roble*, 1984*a*, *b*;

[1]Now at Center for Atmospheric Research, University of Lowell, Lowell, Massachusetts.

Paper number 89JA01549.
0148-0227/89/89JA-01549$05.00

Unclassified
SECURITY CLASSIFICATION OF THIS PAGE

REPORT DOCUMENTATION PAGE

Form Approved
OMB No. 0704-0188

1a. REPORT SECURITY CLASSIFICATION Unclassified	1b. RESTRICTIVE MARKINGS
2a. SECURITY CLASSIFICATION AUTHORITY	3. DISTRIBUTION/AVAILABILITY OF REPORT Approved for public release; Distribution unlimited
2b. DECLASSIFICATION/DOWNGRADING SCHEDULE	
4. PERFORMING ORGANIZATION REPORT NUMBER(S) GL-TR-90-0109	5. MONITORING ORGANIZATION REPORT NUMBER(S)
6a. NAME OF PERFORMING ORGANIZATION Geophysics Laboratory 6b. OFFICE SYMBOL (If applicable) LIS	7a. NAME OF MONITORING ORGANIZATION
6c. ADDRESS (City, State, and ZIP Code) Hanscom AFB Massachusetts 01731-5000	7b. ADDRESS (City, State, and ZIP Code)
8a. NAME OF FUNDING/SPONSORING ORGANIZATION 8b. OFFICE SYMBOL (If applicable)	9. PROCUREMENT INSTRUMENT IDENTIFICATION NUMBER
8c. ADDRESS (City, State, and ZIP Code)	10. SOURCE OF FUNDING NUMBERS PROGRAM ELEMENT NO: 61102F; PROJECT NO: 2310; TASK NO: G9; WORK UNIT ACCESSION NO: 03

11. TITLE (Include Security Classification)
Thermospheric Dynamics During September 18-19, 1984 1. Model Simulations

12. PERSONAL AUTHOR(S)
G. Crowley*[1], B.A. Emery*, R.G. Roble*, H.C. Carlson, Jr., D.J. Knipp**

13a. TYPE OF REPORT	13b. TIME COVERED	14. DATE OF REPORT (Year, Month, Day)	15. PAGE COUNT
Reprint	FROM _____ TO _____	1990 May 4	20

16. SUPPLEMENTARY NOTATION *High Altitude Observatory, National Center for Atmospheric Research Boulder, Colorado (1-Now at Center for Atmospheric Research, University of Lowell, MA) ** Physics Department, USAF Academy, Colorado Springs, CO - Reprinted from Journal of Geophysical Rsch, Vol. 94, No. A12, pp 16,925-16,944, December 1, 1989

17. COSATI CODES		
FIELD	GROUP	SUB-GROUP

18. SUBJECT TERMS (Continue on reverse if necessary and identify by block number)
Thermosphere, Ionosphere-Thermosphere, Global Dynamics

19. ABSTRACT (Continue on reverse if necessary and identify by block number)

For realistic predictions of global thermospheric dynamics using thermospheric general circulation models (TGCMs), one of the main problems lies in the specification of the three-dimensional, time-dependent forcing fields for any given day. The September 18-19, 1984, Equinox Transition Study (ETS) interval was simulated using the National Center for Atmospheric Research TGCM with inputs guided by observations. During the ETS campaign, large quantities of high-quality data were available from high latitudes, and the high-latitude forcings for the TGCM could therefore be defined with precision for this period. The importance of upward propagating semidiurnal tides is also emphasized. This is the first realistic time-dependent simulation to incorporate upward propagating tides. Magnetically quiet conditions prevailed for several days prior to the magnetic storm which began about 0930 UT on September 19, 1984. The storm generated major disturbances in the global circulation, temperature, and composition of the thermosphere. A description of the simulated quiet time thermospheric structure for September 18 is contrasted with the storm time behavior on September 19. Several features of the storm response are described, including the generation of large-scale equatorward propagating disturbances. Longer-lived perturbations of the neutral temperature and composition are also discussed. A new feature has been discovered in the model predictions for altitudes around 200 km. This feature comprises a quasi-fixed four-cell pattern of high- and low-density regions in the polar cap. The exact location of the feature varies with UT, and the magnitude of the density perturbations depends on the strength of the high-latitude convection.

20. DISTRIBUTION/AVAILABILITY OF ABSTRACT
☐ UNCLASSIFIED/UNLIMITED ☒ SAME AS RPT. ☐ DTIC USERS

Unclassified

22a. NAME OF RESPONSIBLE INDIVIDUAL	22b. TELEPHONE (Include Area Code)	22c. OFFICE SYMBOL
H.C. Carlson, Jr.	(617) 377-2458	LIS

DD Form 1473, JUN 86 *Previous editions are obsolete.* SECURITY CLASSIFICATION OF THIS PAGE
Unclassified

Sipler et al., 1981, 1983; *Meriwether et al.*, 1984; *Sica et al.*, 1986*a*, *b*; *Rees et al.*, 1980, 1984, 1986]. In addition, various wave models have also been developed to study the propagation of aurorally generated disturbances [e.g., *Mayr et al.*, 1984*a*, *b*].

To obtain realistic predictions of global thermospheric dynamics using TGCMs, one of the main problems lies in the specification of the three-dimensional, time-dependent, forcing fields for any given day. The usual high-latitude input models represent average conditions obtained from many days of data and cannot be expected to accurately reproduce the appropriate inputs for any specific day. To date, little effort has been made to reduce the number of free parameters in the thermospheric models (by reference to large quantities of data) and then to accurately simulate conditions at a large number of locations simultaneously. *Roble et al.* [1987] recently simulated the thermospheric response to the magnetic storm of March 22, 1979. *Roble et al.* [1988] also simulated a second interval close to solar maximum: November 21–22, 1981, a period of steady magnetospheric forcing. Both of these studies resulted in areas of agreement and disagreement between the TGCM predictions and various data sets, and both identified problems in defining the high-latitude convection pattern for specific days.

In the present study, the NCAR TGCM has been used to simulate the ETS campaign core period of September 18–19. The thermospheric simulations presented in this paper represent the "state of the art" for time-dependent modeling, in that new and improved formulations have been used for the convection and particle precipitation inputs, and the effects of upward propagating semidiurnal tides have been included. The arbitrary adjustment of input variables in order to obtain thermospheric predictions which match measurements was avoided in this study. Details of the TGCM inputs are described below.

For the quiet day (September 18) the effects of both tides and high-latitude forcing on the global thermospheric morphology are illustrated. The storm day behavior is then contrasted with the quiet day, emphasizing the increased importance of the high-latitude forcing. In a companion paper [*Crowley et al.*, this issue] the TGCM predictions are compared with data from many locations, including incoherent scatter radars, ionosondes, and a satellite accelerometer. The validity of the TGCM predictions is assessed on a statistical basis, and the general utility of such predictions is discussed.

2. GEOPHYSICAL CONDITIONS FOR SEPTEMBER 18–19, 1984

The solar $F_{10.7}$ flux was very low and typical of solar minimum conditions, although the true solar minimum did not occur until late 1985, more than a year later. Figure 1 illustrates the variation of the *Kp* and *Dst* indices for September 17–21, 1984. The geomagnetic storm that began on September 19, 1984, was "isolated" in the sense that the storm was preceded by several days of very quiet conditions and followed by a moderately quiet day. *Kp* had values of less than 3o from 00 UT on September 16 until 09 UT on September 19, at which time it rose from 2+ to 6o and remained at least 4o or above for 24 hours. Similarly, the *Dst* index remained in the range −2 nT to +12 nT from September 13 to 15 UT on September 18. Between 00 and 05 UT on

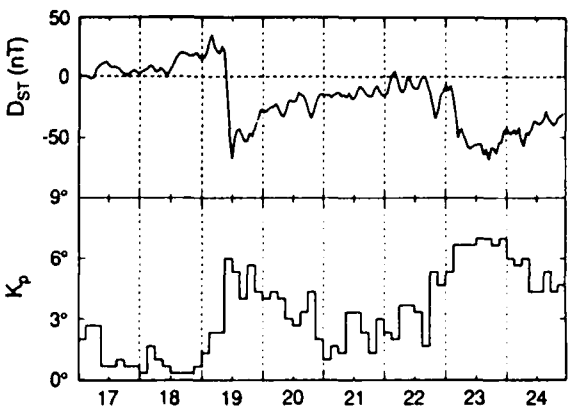

Fig. 1. Variation of magnetic *Dst* and *Kp* indices for the Equinox Transition Study of September 17–24, 1984.

September 19, the *Dst* index increased decisively from +15 nT to +30 nT before plunging to −67 nT at 12 UT. Recovery of the *Dst* index to small negative values occurred over the next 60 hours, with *Kp* returning to low levels at the end of September 20. This magnetic storm was not associated with a sudden commencement (sc) and therefore belongs to the class known as gradual onset storms.

Figure 2 presents the *AE* and hemispheric power (*Hp*) indices for September 19. These indices have a higher time resolution than the *Kp* or *Dst* indices. The main features of the *AE* index are three large substorms commencing around 0930, 1500, and 1800 UT. The *AE* index rises from 100 nT at 09 UT to more than 1000 nT by 11 UT. The *Hp* index [*Fuller-Rowell and Evans*, 1987] has less variability than the *AE* index and does not appear to track individual substorms, although the general increase of activity is evident after 09 UT. Also shown in Figure 2 are the cross-polar cap potential difference and Joule heating obtained from the assimilative mapping of ionospheric electrodynamics (AMIE) technique [*Knipp et al.*, this issue]. The potential and Joule heating display large variations which are well correlated with the variations in *AE*. The potential on September 19 remained above 100 kV for 2 hours from 1030 to 1230 UT and reached a maximum value of about 160 kV. The ionosphere never regained a quiescent state between substorms, and the substorms were superposed on a generally increased level of activity. To summarize, the ETS interval represents a geomagnetically variable period with close to solar minimum conditions. The work described here thus makes a particularly interesting contrast with the work of *Roble et al.* [1987], who studied a magnetically active equinox interval for solar maximum conditions.

3. SPECIFICATION OF TGCM INPUTS

General details of the inputs required by the TGCM have been described in the papers listed in the introduction. A diurnally reproducible TGCM solution for the prestorm conditions of September 17, 1984, was obtained prior to any attempt at modeling the ETS interval. The diurnally reproducible solution assumed a time-invariant ionospheric convection pattern with a cross-polar cap potential drop of 20 kV and a small auroral oval with the total power input from particle precipitation of 2×10^{10} W. The TGCM time step

A-1 20

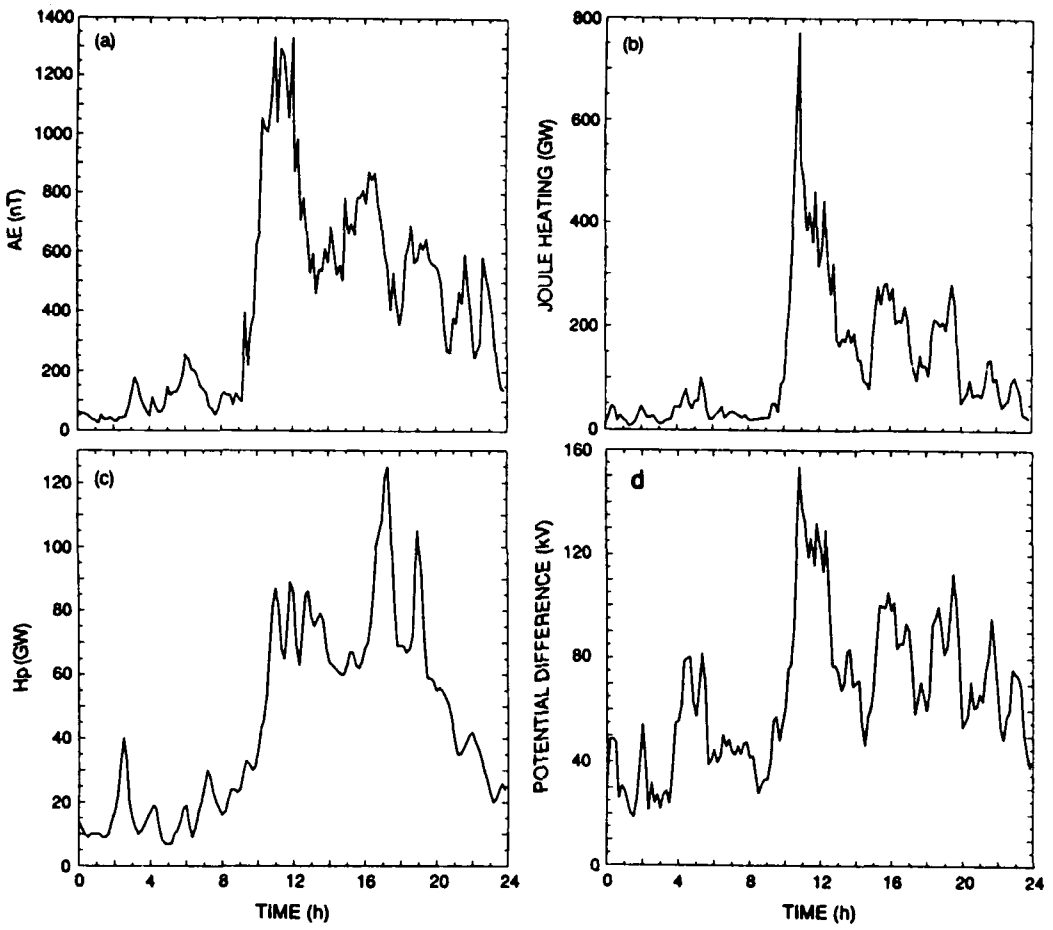

Fig. 2. Variation of geophysical indices and electrodynamic parameters for September 19, 1984. (*a*) *AE* index (minute values) for September 19, 1984, showing detailed development of substorm activity. (*b*) Hemisphere power index (supplied by D. S. Evans, NOAA). (*c*) Joule heating integrated over northern hemisphere obtained from AMIE technique [after *Knipp et al.*, this issue]. (*d*) Potential difference from AMIE technique [after *Knipp et al.*, this issue].

for the entire simulation was 2½ min, and linear interpolation was used to obtain input values at a given time step. Specific features of the inputs employed in the simulations for the ETS interval will now be described.

3.1. *Ionospheric Convection*

For realistic simulation of polar thermosphere dynamics by the NCAR TGCM during magnetically disturbed periods, the spatial distribution and temporal evolution of high-latitude electric fields must be accurately defined. Normally, the high-latitude convection pattern is not available, and a representative pattern must be substituted. Early studies of global thermospheric dynamics employed simple patterns such as the *Volland* [1978] model. More recently, the *Heelis et al.* [1982] model has been adopted, as described by *Roble and Ridley* [1987].

Roble et al. [1987, 1988] have recently compared time-dependent TGCM predictions with various data sets and identified problems in defining the high-latitude convection pattern using the Heelis model. Similar difficulties were encountered for the ETS simulation, in manually tuning the Heelis model to match numerous electric field observations. In general, tuning of the convection pattern for one longitude sector does not yield improvements in other sectors.

The fitting of large quantities of data is a task more suited to a computer algorithm than a manual technique. The AMIE technique of *Richmond and Kamide* [1988] and *Richmond et al.* [1988] was therefore adopted for this purpose for September 19. The AMIE algorithm has the further advantage that many different types of data may be assimilated to derive the final convection pattern. The derivation of potential patterns for the ETS interval from large quantities of data in the northern hemisphere is discussed in detail by *Knipp et al.* [this issue]. The patterns were obtained with a 10-min time resolution and are thought to be the most realistic representation of the ETS convection patterns currently possible.

Throughout the day, the shape and size of the convection pattern changes on time scales of less than 1 hour. Figure 3 depicts potential patterns for 09, 11, 12, and 18 UT on the storm day. Around 09 UT, prior to the storm onset, the evening cell completely dominates the morning cell, and drift velocities are generally less than 300 m s^{-1}. The morning cell is dominant around 11 UT and 12 UT and contains drift velocities approaching 2000 m s^{-1}. Around 18 UT the evening cell is again dominant, although the AMIE pattern is somewhat distorted in the late morning sector. This selection of patterns illustrates the complexity of the high-latitude convection and emphasizes the extreme difficulty of manu-

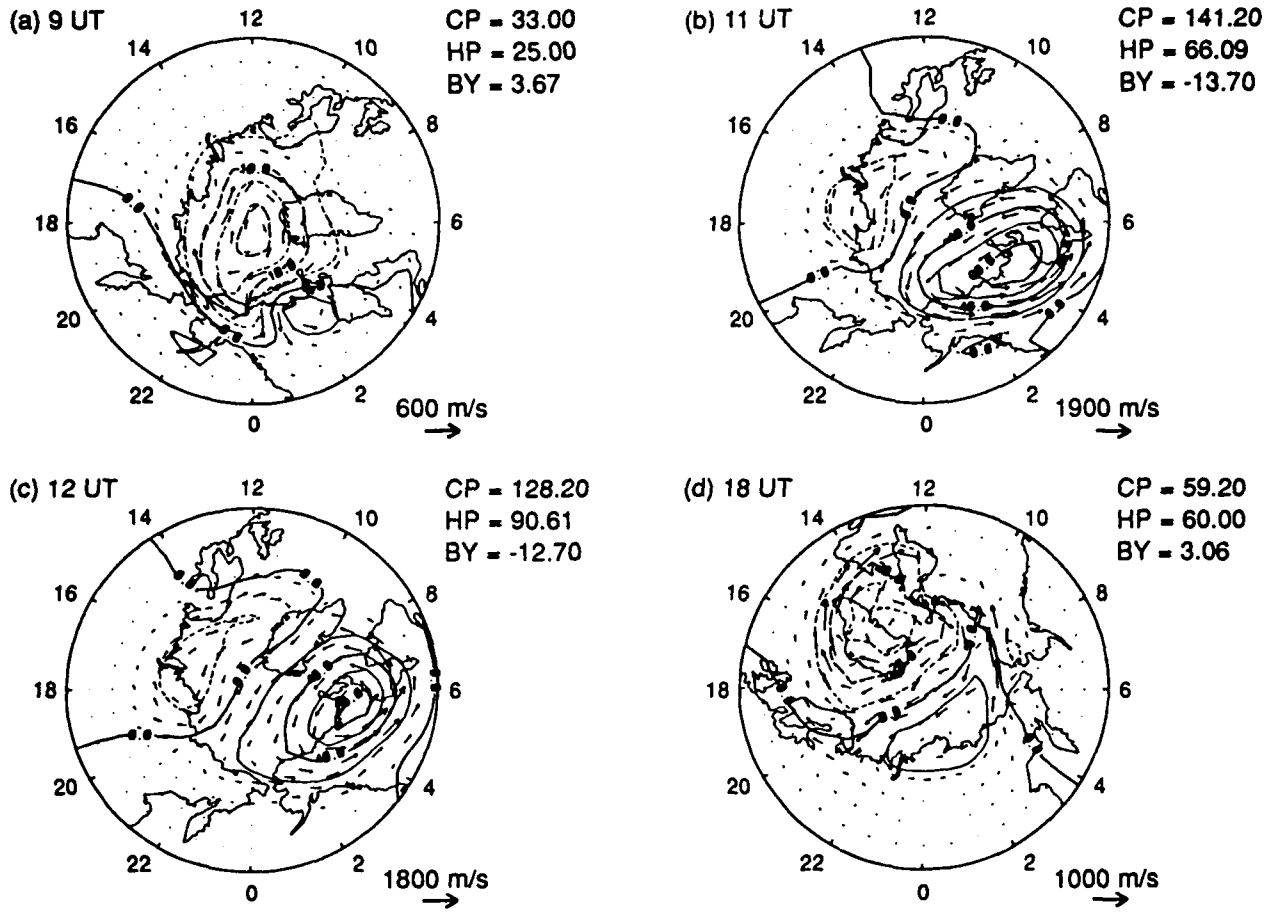

Fig. 3. Snapshots of convection obtained from AMIE technique for northern hemisphere (>50°N) around 09, 11, 12, and 18 UT on September 19, 1984. Arrows indicate convection velocities, and contours depict corresponding potential patterns. The shape, size, and orientation of dawn and dusk cells vary dramatically during the storm period, with maximum velocities approaching 2 km s^{-1}.

ally tuning a simple analytic model such as the Heelis model to obtain realistic instantaneous patterns.

Very few electrodynamic data were available from the southern hemisphere for the ETS interval; therefore the AMIE technique could not be applied there. Furthermore, the potential pattern obtained for the northern hemisphere is inappropriate for the southern hemisphere because of the different B_y dependence of the dawn and dusk convection cells in the two hemispheres. Similarly, a simple inversion of the pattern would place the polar cap entry and exit regions at the wrong local times. For the southern hemisphere we therefore readopted the Heelis model (with B_y dependence). The parameters required as inputs for the Heelis model were deduced from the northern hemisphere AMIE potential patterns and from various parameterizations described by *Emery et al.* [1989]. The northern hemisphere patterns contributed a measure of B_y, cross–polar cap potential, radius of convection, and the falloff rate of the potential equatorward of the convection reversal. Note that defining a southern hemisphere Heelis pattern to approximately match a fully defined convection pattern from the northern hemisphere is relatively simple, although the results for the southern hemisphere are not expected to be as realistic as for the northern hemisphere. This use of the Heelis model in the southern hemisphere was not expected to significantly affect the northern hemisphere simulations or data comparisons; however, waves generated in the southern hemisphere propagate into the northern hemisphere and therefore perturb the thermospheric simulations, as described later.

The AMIE technique is difficult to apply to geomagnetically quiet conditions, such as those on September 18, 1984. This is because the magnetic field inputs to AMIE are deviations from their quiet day values, and on quiet days such as September 18 the measurement errors are comparable with the deviations themselves. We were thus forced to retain the Heelis convection model for both hemispheres on this day. Since the high-latitude heat and momentum inputs were relatively small on September 18, their influence on thermospheric dynamics is not expected to be significant outside the polar cap.

3.2. *Particle Precipitation*

Parameterization of the particle precipitation in the auroral oval, the polar cusp, and polar rain was described in detail by *Roble and Ridley* [1987] and *Emery et al.* [1989]. The parameterizations were designed to give reasonable TGCM inputs for a variety of situations, and by their nature represent average conditions. For the ETS interval a DMSP satellite and two NOAA satellites measured auroral particle

precipitation in different magnetic local time sectors, and data were therefore available to test the validity of the parameterizations. In general, the location of the parameterized oval differed from the measured location.

Numerical experiments revealed that for magnetically active intervals, changes of a few degrees in the location of the precipitation modified the Joule heating and momentum forcing in the model and produced significant variations in the global wind patterns. For the ETS interval, some effort was therefore put into tuning the location of the oval by using the satellite measurements, and a semiautomatic technique was developed, as described by *Emery et al.* [1989].

Figure 4 illustrates an example where the tuning significantly changed the location of particle precipitation in the model, although the effect was less dramatic in most other cases. At about 1412 UT the hemispheric power was 61 GW, and the cross–polar cap potential was 72 kV. Figure 4*a* depicts the auroral oval obtained from the parameterized model for these conditions. The solid radial lines in Figure 4*a* indicate where the DMSP and NOAA satellite measurements of particle energy flux exceeded 0.25 erg cm^{-1} s^{-1}. The dayside measurements are equatorward of the predicted oval.

Tuning of the oval to match the data, as described by *Emery et al.* [1989], yields the result depicted in Figure 4*b*. The radius of the oval has increased by 2°, and its center (0) is offset toward the opposite side of the magnetic pole (P) with respect to the parameterized result.

Although the tuned auroral oval matches the measured oval much better than the parameterization, the simplicity of the model means that details such as narrow or wide auroral regions cannot be reproduced in general. The orbital period of each satellite was about 100 min, and although data were generally available from both hemispheres, coverage was extremely sparse. Neither the temporal nor spatial development of the auroral oval could be reproduced with any great accuracy. For more realistic TGCM inputs, denser data coverage is necessary. The type of images provided by the DE 1 or Viking satellites, which often show the entire auroral oval with a time resolution of about 10 min, might be used in the future if they can be transferred to the TGCM grid and if particle energies and fluxes can be inferred from the data.

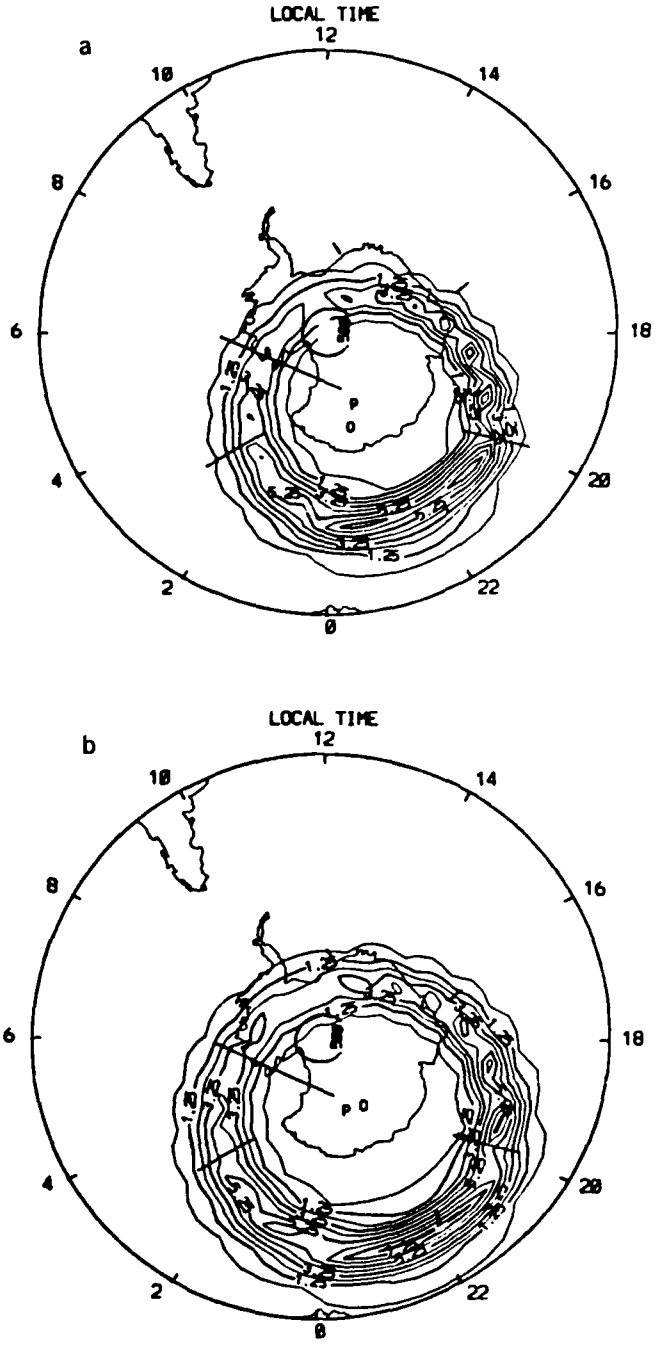

Fig. 4. Comparison of (*a*) parameterized and (*b*) tuned auroral oval in TGCM, for 1412 UT September 19, 1984. Solid radial lines indicate satellite measurements of energy flux exceeding 0.25 erg cm s^{-1}. For a hemispheric power of 61 GW and cross–polar cap potential of 72 kV, the parameterization yielded an auroral radius of 22.4°, with a center (0) offset from the magnetic pole by 4.3° and 1.0° toward the midnight and dawn sectors, respectively. The tuned auroral oval has a radius of 26.2°, and its center (0) is offset from the magnetic pole by 0.8° and 3.3° toward the noon and dusk sectors, respectively.

3.3. *Auroral Particle Energies*

Particle energies are an important consideration for high-latitude dynamics, since the energy determines at what altitude the particles deposit most of their energy and produce most ionization. Two particle populations are of interest here: those with energies <300 eV which deposit their energy above ~180 km, and those with energies >300 eV reaching altitudes below 180 km. Because the Pedersen conductivity peak is below 180 km, the latter population determines the altitude and amount of Joule heating in the model due to enhanced conductivity.

A brief examination of the NOAA and DMSP satellite data for particle energies >300 eV revealed that the particle energies in the parameterized auroral oval model of the TGCM were significantly higher than those observed during the storm. Typically the observed values of 1 keV were modeled by 4-keV electrons in the TGCM. The altitude of maximum ionization in the model would then be ~100 km instead of 120 km, and the contribution to Pedersen conductivity and Joule heating would be much smaller in the model than if the ionization had been correctly deposited at 120 km, which is close to the Pedersen conductivity peak. Thus the particle precipitation model described by *Roble et al.* [1987]

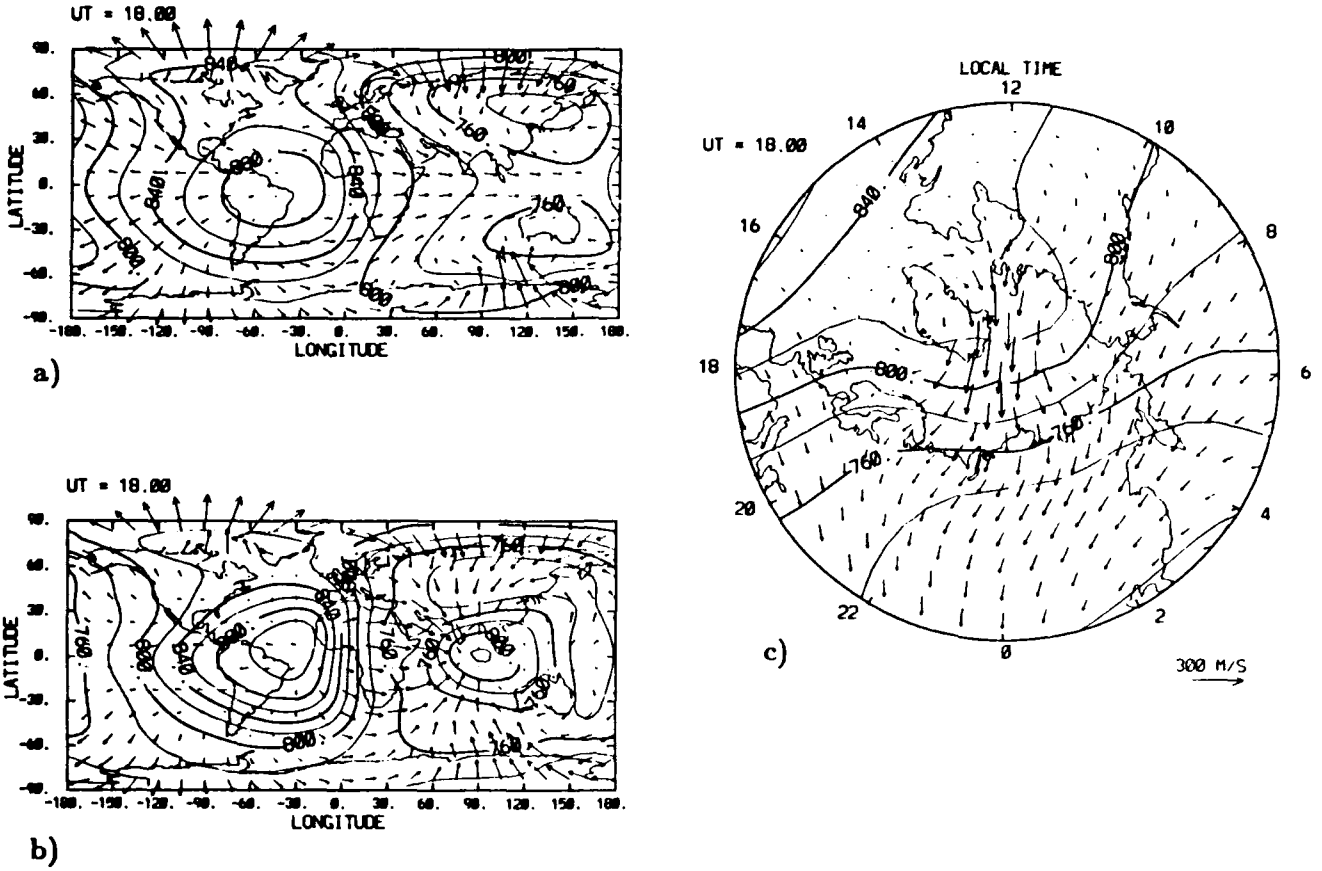

Fig. 5. Quiet day winds and temperatures for $Z = +2$ pressure level at 18 UT, from the NCAR TGCM. (*a*) No tides. (*b*) Tides included. (*c*) Same as Figure 5*b* but only northern hemisphere is depicted in polar coordinates, for latitudes exceeding 40°N. The velocity vector scale is the same for all three frames.

was modified to yield energies consistent with data from the satellites [*Emery et al.*, 1989]. A simple sensitivity study reveals that the global effects of such changes are insignificant during quiet times, but extremely important during magnetically active intervals. A detailed discussion of the effects of varying the particle energies in the TGCM is outside the scope of this paper.

Soft particle precipitation in the TGCM currently includes only the polar rain and polar cusp precipitation [*Roble and Ridley*, 1987]. The heat input per unit mass is greater for low-energy particles because their energy is deposited at higher altitudes, and very significant effects in the *F* region winds can be generated by a small total energy input. An additional soft particle component (~200 eV) was thus invoked by *Smith et al.* [1982] to yield stronger equatorward mid-latitude *F* region winds in the University College London (UCL) three-dimensional thermospheric model. Future versions of the TGCM will include this additional soft particle component in the auroral oval.

3.4. *Background Ionosphere*

Roble et al. [1988] have designed a coupled thermosphere/ionosphere general circulation model (TIGCM) that calculates a self-consistent ionosphere with thermosphere dynamics. This model is presently in a state of development, and in this paper we use an older version of the TGCM in which the ionosphere is specified empirically as described by *Dickinson et al.* [1981]. *Roble and Ridley* [1987] described modifications to the TGCM to account for auroral precipitation in the lower thermosphere that the empirical models do not adequately represent. The auroral electron density enhancements discussed above were added to the densities obtained from the international reference ionosphere (IRI) [*Bilitza*, 1986], and the total electron density was used to calculate ion drag, momentum forcing, and Joule heating terms at each TGCM time step. The IRI ionospheric model provides peak electron densities at approximately correct altitudes, although f_0F_2 is somewhat reduced from the values measured on quiet days during the ETS interval. Consequently, the ion drag would tend to be underestimated in the TGCM. The $O\text{-}O^+$ collision cross section is another important parameter for determining the ion drag. Recent work by *Burnside et al.* [1987] suggests that the $O\text{-}O^+$ collision cross section of *Schunk and Walker* [1973] is too small, and its value was therefore increased by a factor of 1.5 in the present simulation.

3.5. *Upward Propagating Tides*

Semidiurnal tides propagating from the lower atmosphere represent a major influence on the thermosphere, particularly at low altitudes [e.g., *Fesen et al.*, 1986]. Tides were ignored in the two solar maximum simulations mentioned above. Since they are important, they have been included in

the present simulation using the specifications of *Fesen et al.* [1986] for equinox solar minimum conditions.

4. RESULTS OF THE SIMULATION

4.1. *Upper Thermosphere*

Having described the TGCM inputs for the September 18–19 ETS interval, the results of the simulation will now be described in detail. Presentation of the quiet day (September 18, day 262) morphology provides a context for the storm time (September 19, day 263) results. The effects of tides on the thermosphere during the quiet period are discussed briefly in order to isolate tidal effects from those due to the magnetic storm.

Winds and temperatures. The quiet day global variations of neutral winds and temperatures predicted for 18 UT on the $Z = +2$ pressure level (altitude of about 300 km) are shown in Figure 5. Figure 5*a* was obtained from a simulation which excluded upward propagating semidiurnal tides, while tidal effects were included in Figures 5*b* and 5*c*. In the absence of tides (Figure 5*a*) the main features of the temperature variation are a day-night asymmetry, with a maximum afternoon temperature 150 K hotter than the minimum nighttime temperature. The winds display the well-known propensity to blow from the dayside high-temperature bulge toward the cold midnight sector. The postmidnight equatorial temperatures are enhanced by about 20 K because of compression associated with convergence of the nighttime meridional neutral winds.

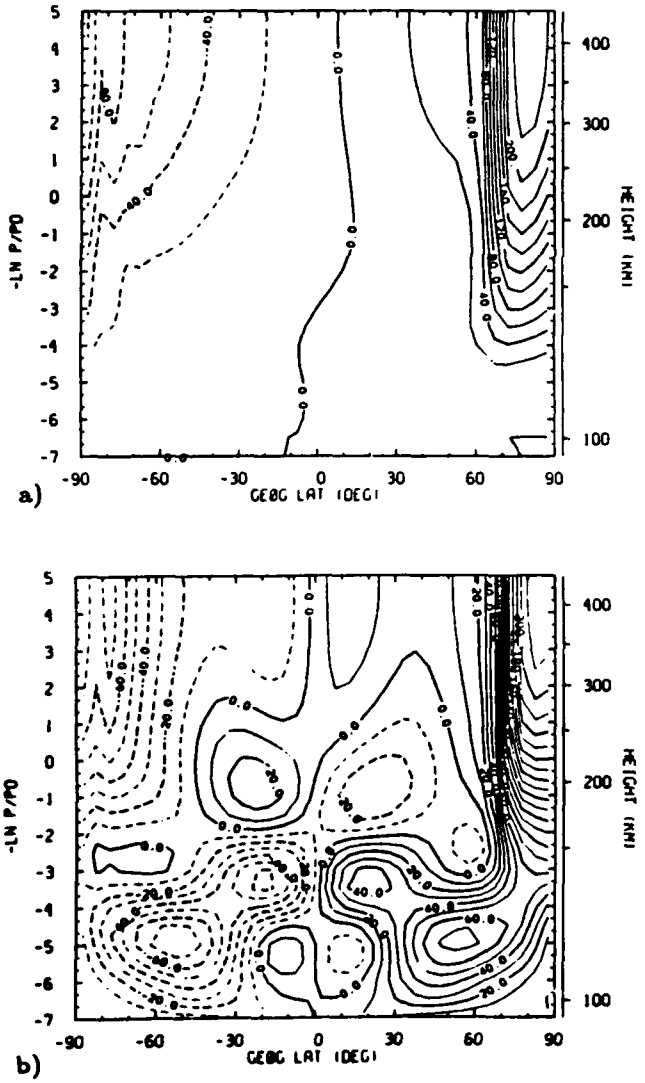

Fig. 6. Latitude versus pressure level slices showing variation of meridional neutral wind for 70°W at 18 UT on a quiet day. (*a*) No tides. (*b*) With tides. Solid contours indicate winds blowing toward the south; dashed lines indicate northward winds. The contour interval is 10 m s^{-1}.

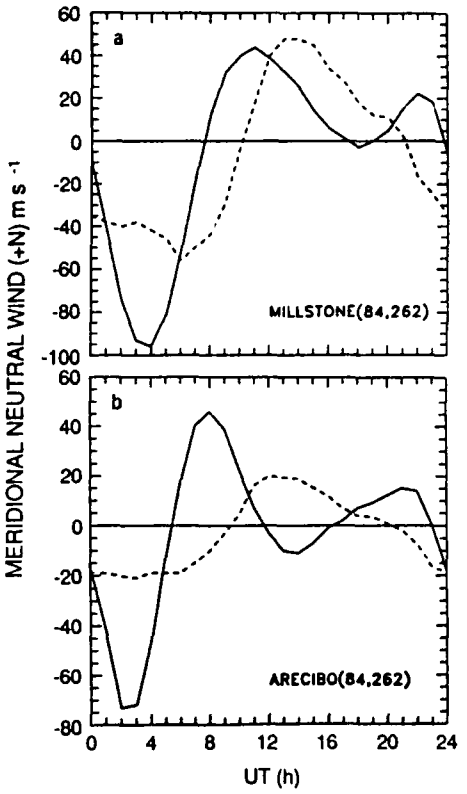

Fig. 7. Variation of meridional neutral wind for 300 km at (*a*) Millstone Hill and (*b*) Arecibo on quiet day (1984, day 262), predicted by the NCAR TGCM. Dashed line indicates no tides; solid line shows effect of including tides.

Inclusion of the upward propagating semidiurnal tides in the simulation (Figures 5*b* and 5*c*) considerably complicates the thermospheric response at the $Z = +2$ level. At low latitudes the tides generate a 20-K enhancement in the dayside temperatures, and the midnight temperatures are about 50 K hotter than in the absence of tides. A similar result was obtained by *Fesen et al.* [1986]. The "midnight temperature bulge" has been discussed in detail by *Spencer et al.* [1979] and more recently by *Herrero et al.* [1985].

The neutral wind response is also modified by the inclusion of tides in the simulation. This modification is illustrated for 18 UT by reference to Figure 6, which depicts the meridional neutral wind structure with and without tides for the 70°W longitude sector. In the case of no tides (Figure 6*a*) the structure is very simple, with poleward winds at all latitudes and altitudes. The upward propagating tides result in a complex wind structure (Figure 6*b*), which includes reversals of the wind direction. Figure 7 illustrates the effect

of tides on the meridional neutral wind at two locations (Millstone Hill and Arecibo) in the 70°W longitude sector. In the absence of tides the winds for Millstone and Arecibo display a strong diurnal variation. The introduction of tides into the simulation superposes a very strong semidiurnal variation in the winds at both locations.

Figure 5*c* depicts a polar view of the quiet time northern hemisphere. The polar cap winds driven by convection are clearly visible in this plot, and they provide an additional perturbation on the features described above. Strong antisunward winds are obtained in the center of the polar cap. In the dusk sector, sunward winds are visible, driven by the auroral return flow in the convection pattern. No sunward flow is obtained in the dawn sector because of weaker ion drag coupling and the fact that the Coriolis force tends to throw the winds equatorward in this sector [*Fuller-Rowell et al.*, 1984; *Killeen and Roble*, 1984, 1986]. During quiet times the high-latitude wind speeds are typically 200 m s^{-1}. Distortion of the temperature contours over the polar cap is also visible in this plot, with high-temperature contours extending into the polar cap from the dayside.

During magnetically active conditions, high-latitude forcing becomes much more important and may even dominate the global thermospheric morphology. The TGCM-calculated neutral winds and temperature pattern on the model $Z = +2$ constant pressure surface (near 300 km) are shown in Figures 8*a*–8*e* for five different universal times on the active day: 09, 12, 13, 18, and 23 UT, respectively. The circulation pattern shown at 09 UT in Figure 8*a* is for the last hour prior to onset of the magnetic storm. The wind and temperature variations are very similar to those described in Figure 5*c*, but the convection-driven winds are displaced further into the nightside at 09 UT since the convection pattern moves around the geographic pole as a function of universal time, due to the offset magnetic pole.

After the onset of the magnetic storm, high-latitude effects begin to dominate the global wind and temperature variations. Expansion of the convection pattern and auroral oval are associated with enhanced Joule heating and momentum forcing. At 12 UT, winds exceeding 300 m s^{-1} are obtained throughout much of the nightside, and speeds of 600 m s^{-1} are generated in the polar cap. Convection effects are so strong that sunward winds are produced in the dawn sector at high latitudes while at lower latitudes, winds generated by Joule heating blow strongly equatorward. Temperatures in the polar cap and auroral zone have increased dramatically and exceed the normal daytime low-latitude maximum temperature of 900 K noted in Figure 5. In addition, the sudden increase of high-latitude forcing generates propagating disturbances. The low-temperature region equatorward of the nightside auroral zone, and the higher-temperature region at lower latitudes, are both associated with a global scale disturbance which is propagating equatorward. By 13 UT the low-temperature region associated with the disturbance has reached latitudes of about 30° on the nightside. Winds at low and middle latitudes are everywhere equatorward, driven by the pressure gradient from high to low latitudes. The temperature contours at this time are extremely complex, because of the presence of various propagating disturbances and localized regions of heating.

At 18 UT on the storm day the temperature and wind variations have relaxed somewhat and are much less chaotic, although the cross–polar cap potential is still around 65 kV (Figure 2). The high-latitude temperatures are generally about 100 K above their quiet time values (Figure 5), and the winds remain at about 500 m s^{-1} in the polar cap and in the evening cell. An interesting high-temperature feature has also developed in the American sector, close to the throat of the dayside convection pattern. This feature corresponds to the dayside temperature maximum noted by *Roble et al.* [1987] in their study of a magnetic storm close to solar maximum. Air parcels having relatively high temperatures are brought to this region particularly from the dusk auroral zone. This process continues as the convection pattern moves round the geographic pole and results, in the present case, in an apparent corotation of the high-temperature feature over the American sector for several hours. By 23 UT (Figure 8*e*) the high-latitude forcing has diminished, and the high-temperature region over the United States becomes isolated, to decay over the next few hours. The winds have also subsided from storm time values, but the polar cap temperatures remain 100 K above the quiet time levels.

It is interesting to compare these predictions with the extreme results of *Roble et al.* [1987] for solar maximum. *Roble et al.* [1987] obtained maximum polar cap winds of 1400 m s^{-1} compared to the present 600 m s^{-1}. They also obtained localized polar cap temperature enhancements of 1000 K, and even 5 hours after the peak of their storm the mean polar cap temperature enhancement was still about 500 K. In the present case, a localized enhancement of 300 K was obtained, and at 23 UT, 4–5 hours after the main activity, the mean polar cap temperatures are only 100 K above their quiet time levels. These differences probably arise from differences in the momentum and Joule heat sources in the two studies, which in turn arise from differences in the convection drifts and electron densities.

Heights. *Rishbeth et al.* [1985] point out the important difference between constant height and constant pressure surfaces. In this paper, constant pressure surfaces are generally used; however, to give some idea of the height variations involved, Figure 9 illustrates the variation of height with latitude for the northern hemisphere $Z = +2$ surface (the southern hemisphere is very similar). Polar plots are used to clarify the high-latitude effects since they are more extreme than the low-latitude effects. In the present sunspot minimum case, the $Z = +2$ pressure level corresponds to altitudes close to 300 km. In contrast, at solar maximum, the $Z = +1$ pressure level corresponds to about 300 km [*Roble et al.*, 1987].

The heights at a constant pressure level are most sensitive to underlying temperature variations; therefore the patterns illustrated in Figure 9 are for the same times as the temperature plots of Figure 8. Tidal effects are visible in the prestorm case for 09 UT (Figure 9*a*). At low latitudes the semidiurnal height variation has extremes at 16 LT (310 km) and 21 LT (285 km) and resembles the semidiurnal temperature variation of Figure 5*c*. High-latitude heating effects also distort the day-night height variation in Figure 9*a*.

By 12 UT the storm is well developed, and the height contours are their most distorted, with altitudes ranging from 342 km in the high-temperature region over Greenland to 290 km in the low-temperature low-latitude region at 21 LT. At 13 UT the height contours are also very distorted, but the minimum height of 280 km is now associated with a low-temperature region of the auroral zone, while the maximum

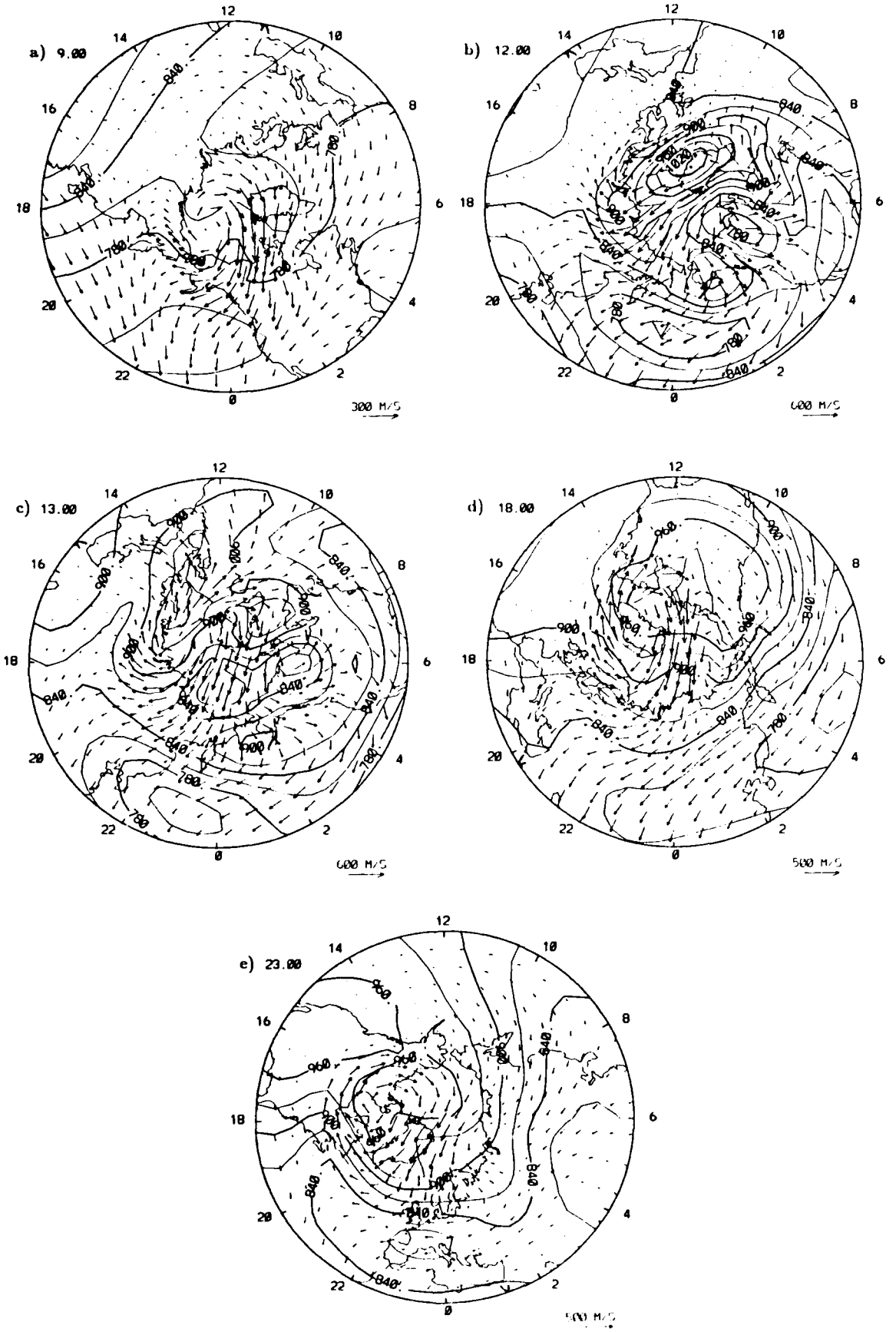

Fig. 8. TGCM-calculated neutral winds and temperatures on the $Z = +2$ pressure level (about 300 km) for (*a*) 09 UT, (*b*) 12 UT, (*c*) 13 UT, (*d*) 18 UT, and (*e*) 23 UT on the storm day September 19, 1984. Latitude range 30°–90°N.

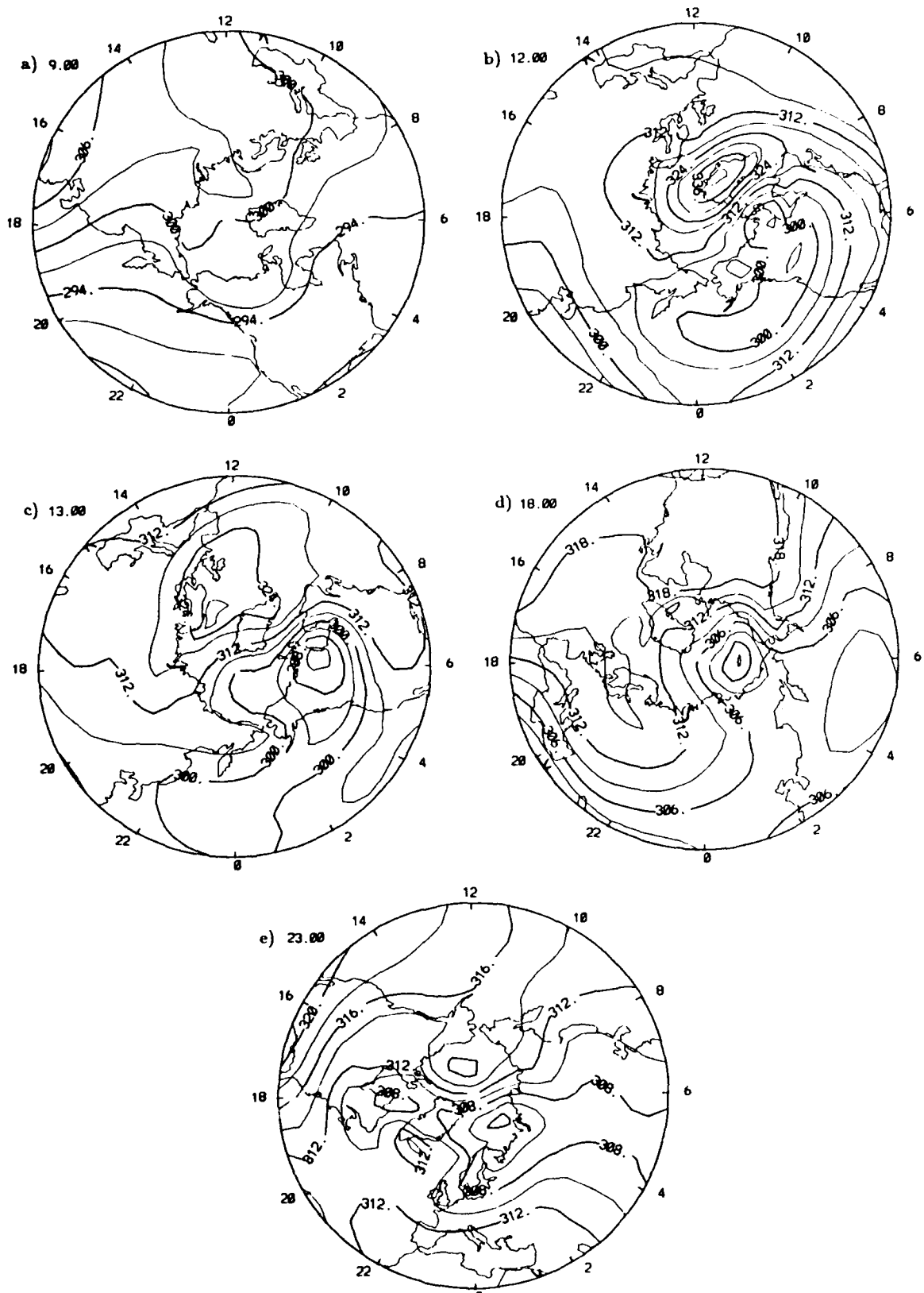

Fig. 9. Height (in kilometers) of the $Z = +2$ pressure surface for the northern hemisphere (>30°N), September 19, 1984, at (*a*) 09 UT, (*b*) 12 UT, (*c*) 13 UT, (*d*) 18 UT, and (*e*) 23 UT.

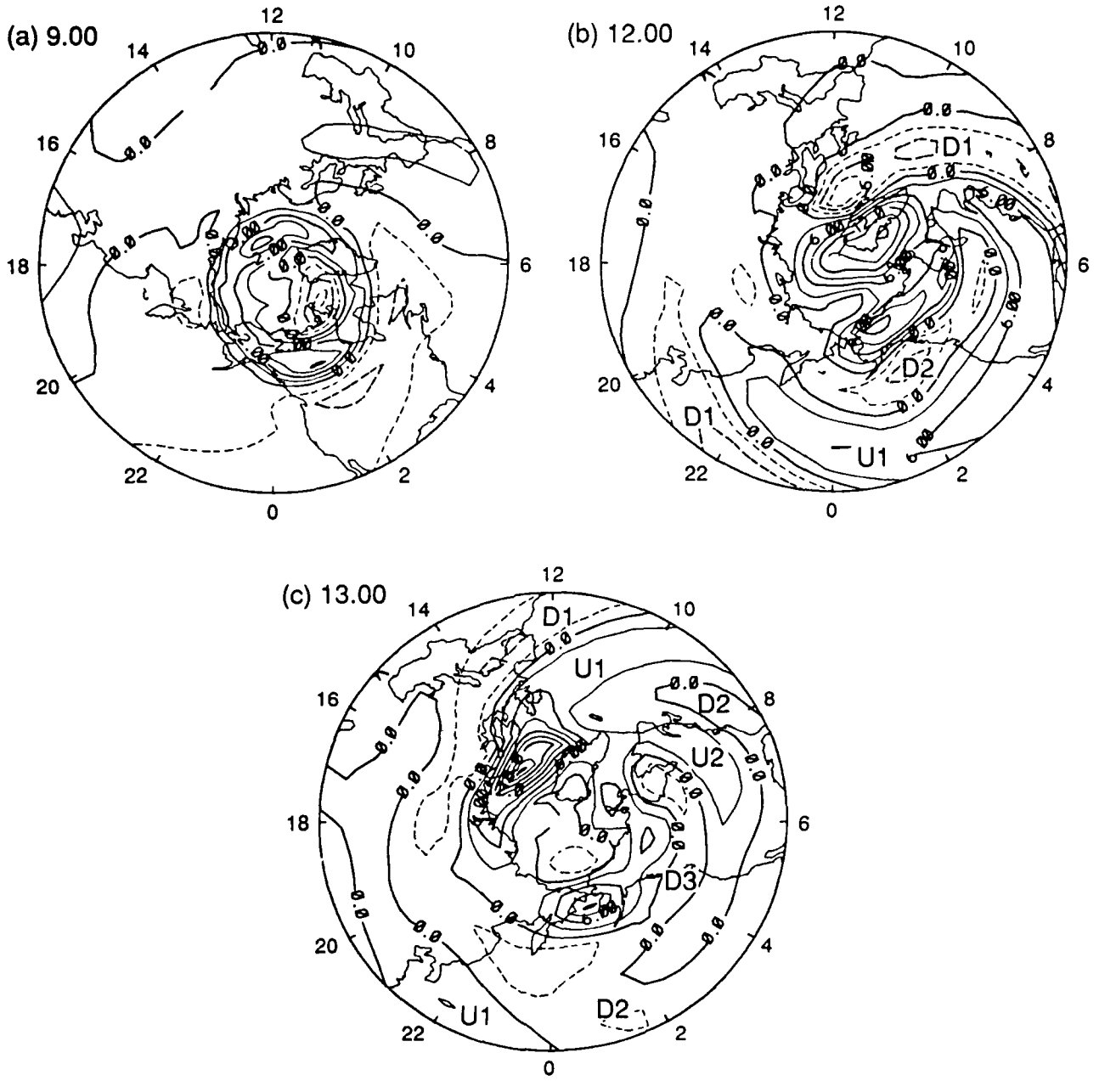

Fig. 10. Vertical winds predicted by the TGCM for the $Z = +2$ pressure level at (*a*) 09 UT, (*b*) 12 UT, and (*c*) 13 UT for September 19, 1984. Solid and dashed contours represent upward and downward winds, respectively. D1, U1, etc., indicate regions of downward and upward winds associated with propagating disturbances.

of 330 km coincides with a propagating disturbance on the dayside.

At 18 UT the low-latitude heights are about 10 km higher than their prestorm values. A broad low-altitude (~300 km) region has also developed at high latitudes. This feature lasted through the end of the day and developed into a four-cell pattern of highs and lows as illustrated in Figure 9*e* for 23 UT. The reason for this feature is not clear, since there are no similar features in the temperature variations of Figures 8*d* and 8*e*. The discussion will return to this feature later in the paper.

Vertical winds. At 09 UT (Figure 10*a*) the vertical wind pattern is typical of quiet times, with downward nighttime winds and upward daytime winds at the lower latitudes. Joule heating in the auroral zone generates upward winds, and in the central polar cap the winds are downward. Typical vertical wind speeds are everywhere less than 5 m s^{-1} and at the lower latitudes 1 m s^{-1}.

The onset of magnetic activity leads to enhanced Joule heating at high latitudes and the generation of propagating disturbances similar to those described by *Roble et al.* [1987]. At 12 UT (Figure 10*b*) a complex wind pattern exists, most of which is due to waves propagating preferentially into the morning sector. A region of downward winds (D1) has

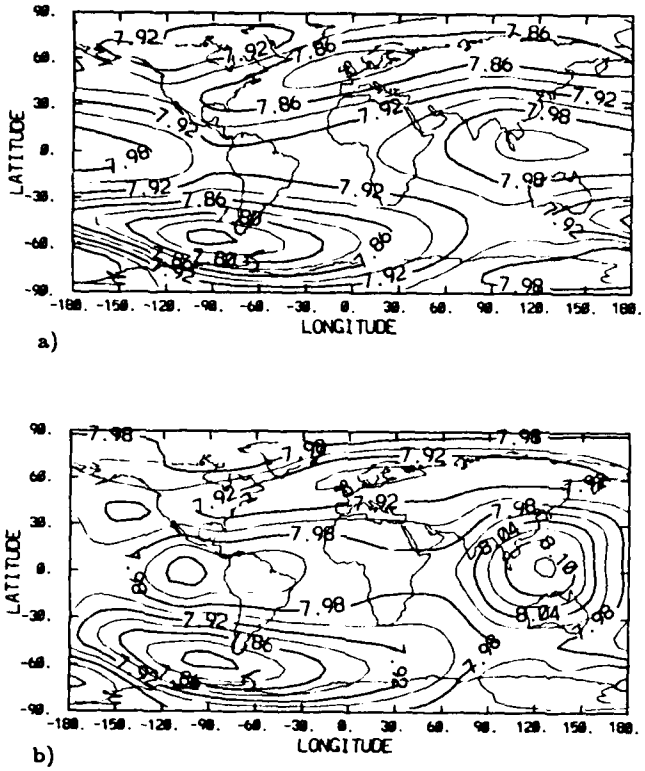

Fig. 11. Global distribution of log N_2 number density for 12 UT at the $Z = +2$ pressure level for the quiet day September 18, 1984. (*a*) No tides. (*b*) With tides.

propagated beyond 27°N in the morning sector, and its extension to other local times virtually encircles the globe. Poleward of this is a region of upward winds (U1), and then more downward winds (D2). In the polar cap/auroral zone, vertical winds of almost 20 m s^{-1} have been generated, and the propagating disturbances contain vertical wind speeds approaching 10 m s^{-1}.

By 13 UT the vertical wind pattern is even more complex. The propagating disturbances D1, U1, and D2 have reached lower latitudes, and further disturbances are identified as U2 and D3. In the auroral zone over northern Europe, vertical winds of 24 m s^{-1} are predicted. Each new injection of energy during the later substorms generates new disturbances which propagate from the high-latitude regions.

Composition. Composition effects during a solar maximum magnetic storm were discussed briefly by *Roble et al.* [1987], in terms of mass mixing ratios. *Rishbeth et al.* [1985] discussed a solstice storm in terms of mean molecular mass. In this paper, number densities will be discussed, together with the ratio of number densities, $O/(O_2 + N_2)$.

The general features of thermospheric composition for quiet conditions were discussed by *Dickinson et al.*[1984]. Some basic points are reiterated here since it is necessary to clarify the origin of several key features. Figures 11*a* and 11*b* compare the global distribution of N_2 with and without upward propagating semidiurnal tides. In the case of no tides a strong diurnal variation of N_2 exists at low latitudes, with the highest (lowest) values of N_2 occurring at dusk (dawn). This diurnal variation is simply due to the diurnal variation of vertical velocity, which is upward during the day and downward at night. There is also a latitude variation, with N_2 being reduced as latitude increases from the equator, until the auroral zone is reached. At high latitudes, N_2 densities again increase because of the effects of upward vertical motion generated by Joule heating in the auroral zone. The inclusion of tides in the simulation (Figure 11*b*) introduces a semidiurnal variation at low latitudes, resulting in N_2 enhancements at both dawn and dusk. In both cases (with and without tides) the minimum value of N_2 density for a fixed pressure level is at subauroral latitudes, and the exact location of the minimum varies with UT as the magnetic pole moves with respect to the geographic pole.

Molecular oxygen O_2 tends to display the same type of variations as N_2, but it is a minor constituent at *F* region altitudes and can essentially be ignored. Atomic oxygen, on the other hand, tends to display the opposite behavior from N_2 and therefore has its maximum value at subauroral latitudes. The atomic to molecular ratio, $O/(O_2 + N_2)$, which is an important parameter in determining *F* region electron concentrations [e.g., *Rishbeth and Garriott*, 1969], thus also has its maximum value for a given pressure level, at subauroral latitudes.

Having established the main features of the quiet time composition variations for *F* region altitudes, we will now address the effects of a magnetic storm on the composition. Figure 12 illustrates the development of the distribution of log N_2 number density for a pressure level of $Z = +2$ in the northern hemisphere during the TGCM simulation for September 19, 1984: 09, 11, 12, and 18 UT (Figures 12*a*–12*d*, respectively). Note that this sequence of times is different from the sequence in Figure 8 to illustrate the composition development most clearly. 09 UT is the last hour before the magnetic storm onset and Figure 12*a* thus represents a quiet time pattern. By 11 UT the auroral oval has expanded, and enhanced Joule heating, especially in the midnight sector, leads to upwelling of N_2 from lower pressure levels. Strong equatorward winds in the post-midnight sector at 11 UT blow down sharp composition gradients and transport nitrogen-rich air to lower latitudes in that sector.

Further upwelling of N_2 and its transport to lower latitudes take place as the storm develops (Figure 12*c*). Corotation tends to be the dominant effect at lower latitudes, and much of the character of Figure 12*d* (18 UT) is due to corotation. The interplay of effects of magnetic activity and corotation between 12 and 22 UT is further illustrated for the $O/(O_2 + N_2)$ ratio by Figure 13. To construct this figure, the global differences between the active and quiet day $O/(O_2 + N_2)$ ratio were obtained for each UT between 12 and 22 UT. The contours representing locations at which no change occurred are plotted in Figure 13. Poleward of these contours, the $O/(O_2 + N_2)$ ratio was diminished during the active day; equatorward the $O/(O_2 + N_2)$ ratio increased. The area of reduced $O/(O_2 + N_2)$ ratio expanded into the morning sector between 12 and 14 UT; however, little energy was injected into the polar cap between 14 and 16 UT (Figure 2), and the established composition features simply tended to corotate. From 16 to 18 UT, more Joule heating occurred, and the same pattern of composition was maintained in spite of corotation effects. From 18 to 20 and from 20 to 22 UT the added Joule heating was not sufficient to cause further significant composition changes at high latitudes; therefore the established pattern simply corotated with the Earth.

Since vertical winds of approximately 1 m s^{-1} produce the quiet time diurnal composition variation, it is clear that the

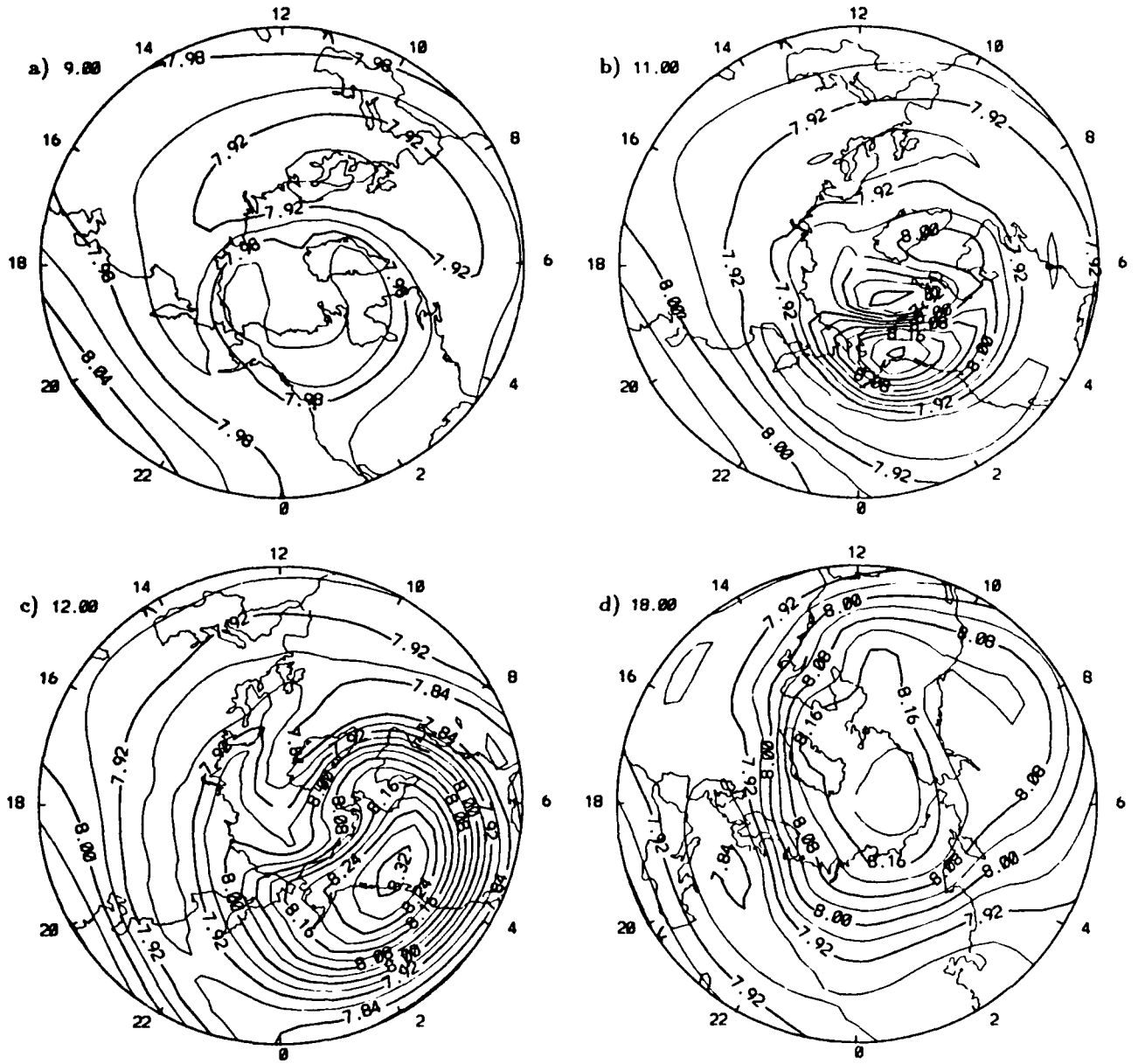

Fig. 12. Development of the distribution of log N_2 number density for the $Z = +2$ pressure level in the northern hemisphere during the TGCM simulation of September 19, 1984: (*a*) 09 UT, (*b*) 11 UT, (*c*) 12 UT, and (*d*) 18 UT.

large vertical winds generated during substorms are capable of producing comparable composition changes but on more rapid time scales of approximately 1 hour. The concept of composition changes caused by storm time vertical winds has been explored by many previous authors. Recently, A. G. Burns et al. (A simulation of thermospheric composition changes for an impulse storm, submitted to *Journal of Geophysical Research*, 1988) analyzed composition changes in the NCAR TGCM for a numerical experiment involving an impulsive "storm" which lasted 3 hours. Perhaps the most interesting concept is that proposed by *Mayr and Volland* [1973] and *Roble et al.* [1977] where a storm time circulation cell drives high-latitude increases of N_2, and a corresponding increase of O at lower latitudes. In the present simulation the predicted composition changes are consistent with the existence of such a circulation system.

Following the onset of magnetic activity, the temperature increases globally, leading to an expansion of the atmosphere and an increase in total gas density for fixed altitudes in the upper thermosphere. At constant pressure levels the storm time conditions refer to greater altitudes (see Figure 9), and the gas density decreases, although at any fixed pressure level the relative concentration of the different gas species is unaffected by the expansion [*Rishbeth and Garriott*, 1969, pp. 8–10]. In the present case, for fixed pressure levels, the value of $[N_2]$ increases at high latitudes and decreases by more than 10% equatorward of the auroral zone. In contrast, the value of [O] decreases at all latitudes, although the magnitude of the decrease is less than 10% equatorward of the auroral zone. Consequently, the atomic to molecular ratio $O/O_2 + N_2$ at the $Z = +2$ pressure level increases equatorward of the auroral zone and decreases at higher latitudes. This implies that some mechanism such as a vertical wind has altered the neutral composition. A

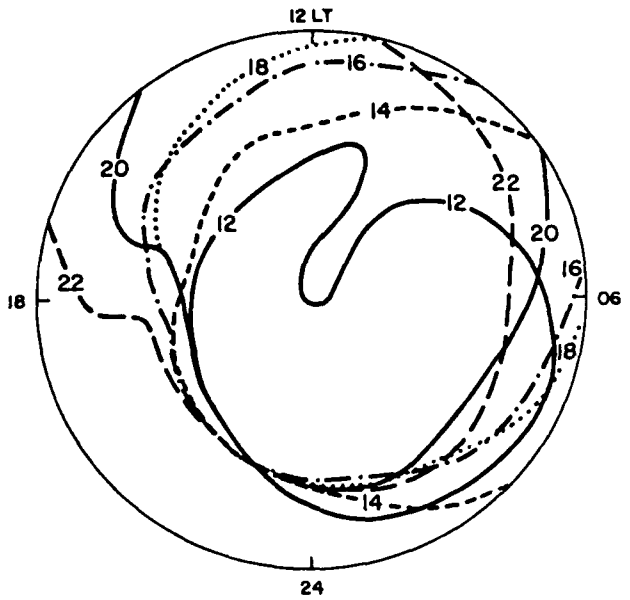

Fig. 13. Polar plot of the northern hemisphere ($Z = +2$) latitudes 30°–90°N in fixed local time coordinates, showing development of contours where quiet day and storm time values of $O/(O_2 + N_2)$ are the same (i.e., zero difference) between 12 and 22 UT. Simple corotation effects would move the pattern anticlockwise by 15° every hour.

relatively stable composition pattern has been established by 13 to 14 UT (Figure 13), which may imply that a stable storm time circulation system has been set up within 3 hours of storm onset.

4.2. *Lower Thermosphere*

The response of the lower thermosphere to the storm is different from that described for the $Z = +2$ pressure surface. Many of the differences between the upper and lower thermosphere have been discussed by *Fuller-Rowell and Rees* [1981], *Roble et al.* [1982, 1983], *Roble and Ridley* [1987], and *Killeen and Roble* [1984]. *Roble et al.* [1987] discussed the lower thermosphere response to an equinox magnetic storm at solar maximum; however, their simulation neglected the effects of upward propagating semidiurnal tides. The tides dominate the quiet time morphology of the lower thermosphere and have been included in the present solar minimum simulation.

In the absence of tides the main features of the global temperature distribution in the lower thermosphere would be a 12-K day-night temperature difference which is perturbed in the polar cap by ±10 K in a two-cell pattern as described by *Roble et al.* [1987]. The neutral winds would blow from the dayside to the nightside. Low-latitude winds would typically be 10 m s^{-1}, with maximum speeds of 75 m s^{-1} antisunward over the polar cap. Typical quiet time results with tides for the $Z = -4$ pressure surface (corresponding to heights of about 120 km) are presented as Figures 14*a*–16*a*. The tides introduce a 70-K semidiurnal temperature variation (Figure 14*a*) with high temperatures at dawn and dusk, and smaller temperatures at noon and midnight. In contrast with the upper thermosphere, the lower thermosphere neutral winds appear to blow from the low-temperature to the high-temperature regions because of the phase properties of the tides. Typical wind speeds are 100 m s^{-1}. There is little evidence of quiet time polar cap temperature and wind effects, because of the dominant effects of tides.

In the absence of tides the $Z = -4$ pressure level corresponds to altitudes of 120–122 km. The tides result in a semidiurnal height variation (Figure 15*a*) between 120 and 123 km. The tides also dominate the quiet time vertical winds (Figure 16*a*) and hence the N_2 number density and composition of the lower thermosphere. The picture of the lower thermosphere presented by *Roble et al.* [1987] which neglected tidal effects is therefore somewhat incomplete and should be regarded as the difference between active and quiet day behavior, bearing in mind the nonlinear nature of the lower thermosphere.

The development of the lower thermosphere storm features in the present case follows a pattern similar to that described by *Roble et al.* [1987]. Enhancement of the high-latitude forcing following storm onset leads to a warm evening cell associated with clockwise wind circulation and a cold morning cell associated with counterclockwise circulation (Figures 14*b*–14*d*). The maximum polar cap temperature perturbations of the storm occurred at 13 UT (Figure 14*c*) and, from an average quiet time temperature of 350 K, reached 420 K on the duskside and 240 K on the dawnside, giving a cross–polar cap temperature gradient of 180 K. This is about half of the temperature gradient obtained by *Roble et al.* [1987]. A second high-temperature feature also developed at mid-latitudes in the morning sector and is thought to result from a combination of tidal effects and adiabatic compression due to the convergence of very strong winds which reached 300 m s^{-1}. These wind speeds are comparable with those obtained by *Roble et al.* [1987] and are large in comparison with quiet day values. The dissipation in the lower thermosphere is small in comparison to that at F region heights, and as a result, once the pattern is spun up during the storm phase, it tends to persist for several hours after the storm has subsided, as noted by *Fuller-Rowell and Rees* [1981] and *Roble et al.* [1987].

The height perturbations closely matched the temperature perturbations at the $Z = -4$ level. The maximum height perturbations during the storm occurred at 13 UT and yielded a cross–polar cap difference of 8 km (Figure 15*b*). This difference had relaxed to 3 km by 23 UT (not shown). Quiet time vertical winds at the $Z = -4$ level are typically ±0.2 m s^{-1}, but during the storm, intense Joule heating in the midnight sector at 11 UT produced upward vertical winds of 4.2 m s^{-1} (Figure 16*b*). This heating also led to the generation of propagating waves, whose manifestation at the $Z = +2$ level has already been discussed. They will be discussed in more detail in a later paper. Prior to the storm the O and N_2 densities are relatively uniform. The storm leads to a negligible change of N_2 and small reduction of O at the $Z = -4$ level, consistent with the change of mass mixing ratio noted by *Roble et al.* [1987].

The mechanisms which produce the two-cell structure in the lower thermosphere at high latitudes have been discussed in detail by previous authors. *Roble et al.* [1982] showed that the high-latitude two-cell convection pattern drives the two-cell lower thermosphere response by momentum coupling. By considering the curl and divergence of the lower thermosphere wind field, they demonstrated that strong upward winds are associated with the vortex which forms on the morningside, and the cold temperatures are due

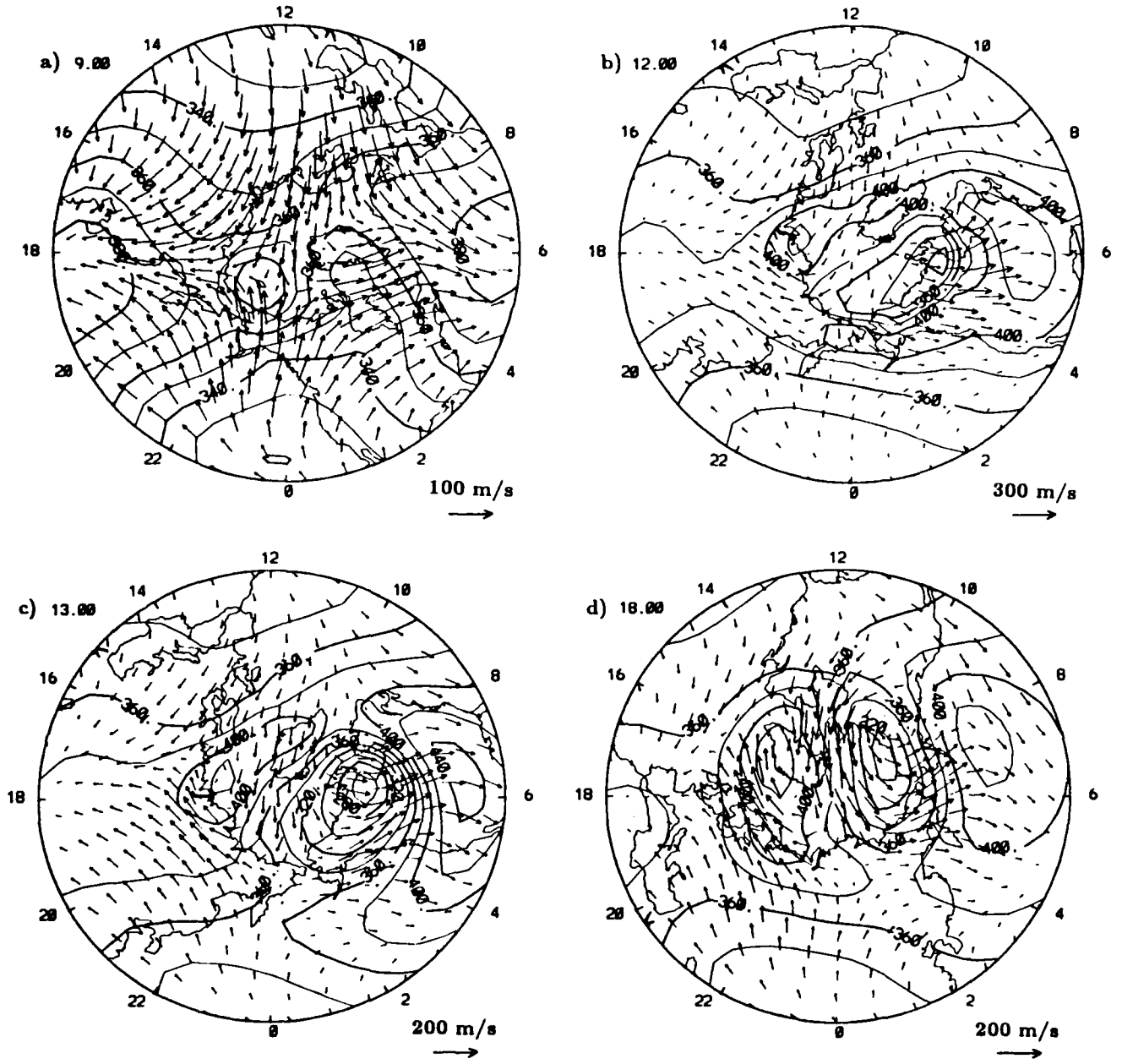

Fig. 14. Development of the wind and temperature distribution for the $Z = +4$ pressure level in the northern hemisphere during the TGCM simulation of September 19, 1984: (*a*) 09 UT, (*b*) 12 UT, (*c*) 13 UT, and (*d*) 18 UT.

to adiabatic cooling. The high temperatures in the evening sector are due to a combination of adiabatic heating and horizontal advection.

The balance of forces which maintains this circulation pattern has been discussed by *Fuller-Rowell and Rees* [1984] and by *Killeen and Roble* [1984]. The intensity of the circulation around the vortices, and the magnitude of the temperature perturbation, depend on the strength of magnetospheric convection. There is also a complex universal time dependence to the circulation and temperature structures as the magnetospheric convection pattern rotates about the geographic pole. The importance of ion drag varies as the convection pattern crosses the terminator and moves alternately into regions of enhanced electron density on the dayside of the polar cap and regions of reduced electron density on the nightside.

A further complication has also been introduced in the present study by the use of realistic convection patterns. In previous studies [e.g., *Roble et al.*, 1982, 1987], simple symmetrical convection patterns have resulted in a lower thermosphere response containing a warm evening cell which was broader than the cold morning cell. In the present study, the relative sizes and orientations of the convection cells varied dramatically (Figure 3). The relative sizes of the resultant vortices in the lower thermosphere were also highly variable as illustrated by Figure 14. For example, at 12 UT (Figure 14*b*) the morning vortex was broader and more intense than the evening vortex. The corresponding

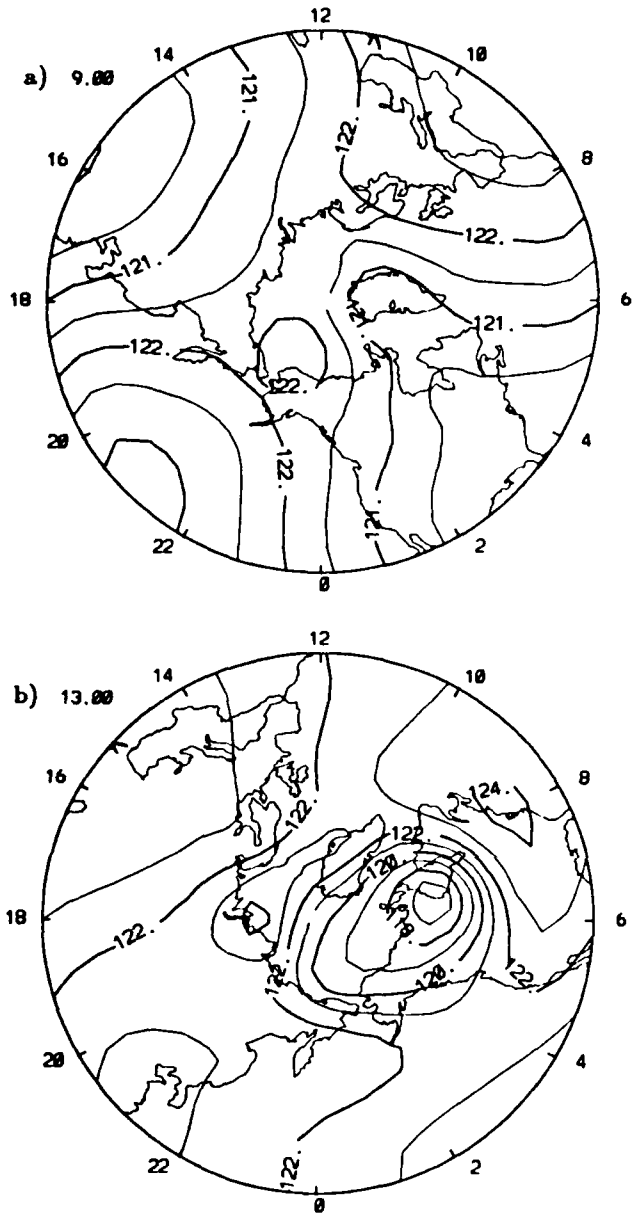

Fig. 15. Height distribution for $Z = +4$ pressure level in northern hemisphere (30°–90°N) from TGCM simulation of September 19, 1984: (*a*) 09 UT and (*b*) 13 UT.

convection pattern (Figure 3*c*) also contained a morning cell which was broader and more intense than the evening cell. On the other hand, at 18 UT (Figure 14*d*) the lower thermosphere temperature distribution and circulation had a dominant evening cell and resembled those of previous studies. The corresponding convection pattern (Figure 3*d*) also had a dominant evening cell. A detailed analysis of the balance of forces in this simulation, such as that provided by *Killeen and Roble* [1984], is outside the scope of this paper. However, this simple analysis further indicates the sensitivity of the lower thermosphere to the details of the high-latitude inputs.

4.3. *Interesting Density Structures in Transition Region (200 km)*

During the ETS interval the S85-1 satellite measured total atmospheric density in an almost circular orbit at altitudes between 197 and 201 km. The TGCM density predictions for fixed altitudes were examined in an attempt to interpret the features in the density measurements. After about 16 UT on the storm day a remarkable feature emerges in the polar cap, as illustrated in Figures 17*b*, 17*c*, and 17*d*, for 16, 17, and 23 UT. The feature consists of a four-cell pattern of alternately high and low densities centered approximately on the magnetic pole, with the highs being approximately Sun aligned. (The extended high-density region at lower latitudes in the dawn sector at 16 and 17 UT is associated with a propagating disturbance and is not part of the high-latitude structure.) The four density cells appear to be closely related to similar features in the height variation. Thus for 23 UT, the density cells (Figure 17*d*) are colocated with the height cells of

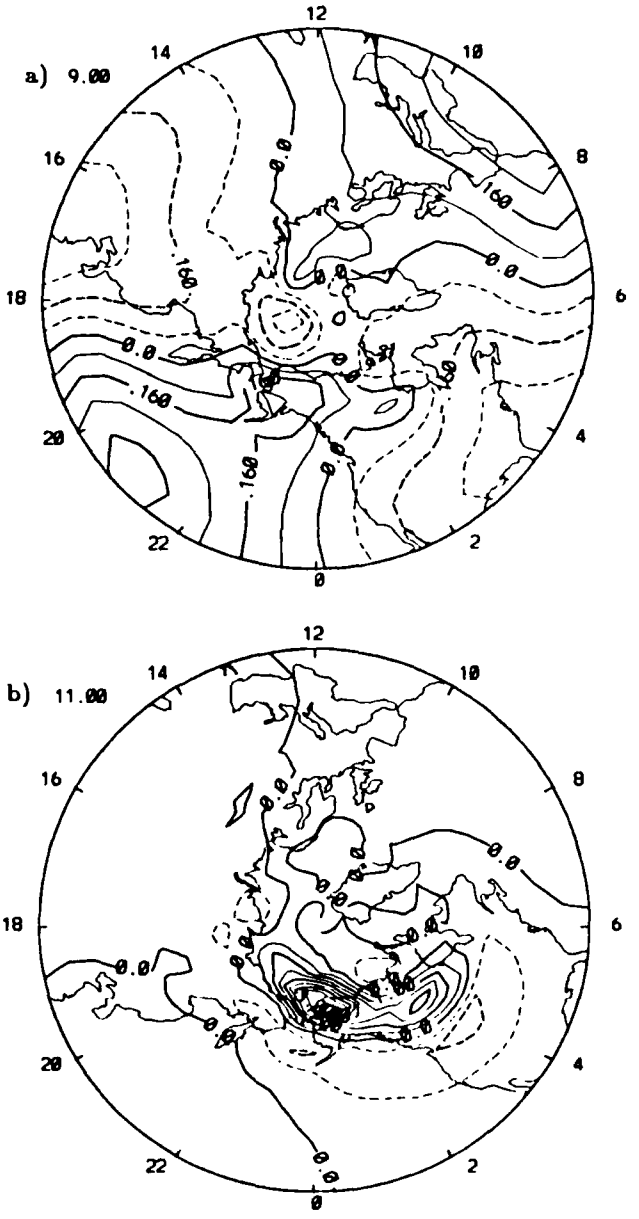

Fig. 16. Distribution of vertical winds at $Z = +4$ pressure level in northern hemisphere (30°–90°N) from TGCM simulation of September 19, 1984: (*a*) 09 UT, contour interval 0.08 m s^{-1}; (*b*) 11 UT, contour interval 0.5 m s^{-1}.

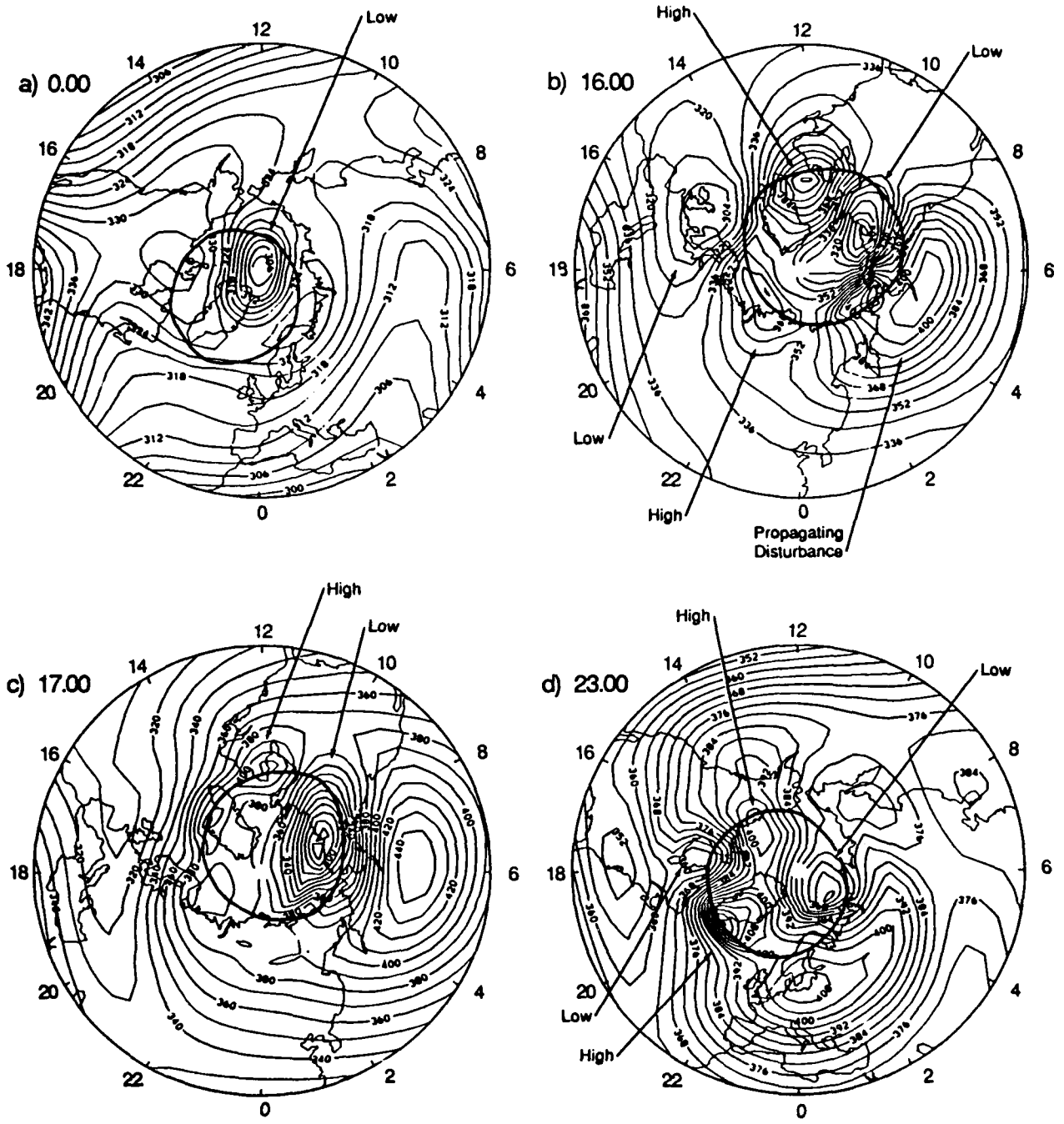

Fig. 17. Development of total mass density ($\times 10^{-15}$ g cm^{-3}) at 200 km for the northern hemisphere (30°–90°N) during the TGCM simulation of September 19, 1984: (*a*) 00 UT, (*b*) 16 UT, (*c*) 17 UT, and (*d*) 23 UT. The main high- and low-density features are labeled appropriately.

Figure 9*c*, and the smaller (greater) densities correspond to lower (higher) altitudes.

An outline of the auroral oval is superimposed on each frame of Figure 17. Because of the offset magnetic and geographic poles the locations of the auroral oval at 16 and 23 UT are very different. In both cases, however, the four-cell density pattern essentially lies within the polar cap and auroral zone, indicating strong geomagnetic control of the feature. The amplitude of the density perturbations depends on magnetic activity, and the most prominent part of the pattern is the low-density region on the dawnside of the polar cap. Thus at 16 UT the amplitude of the perturbations is comparable with the amplitude of the low-latitude tidal effects, while prior to the storm at 00 UT (Figure 17*a*), only the low-density dawn cell is visible.

The existence of this new feature is confirmed by the S85-1 satellite measurements. During the afternoon of September 19, density perturbations measured on three separate satellite passes are colocated with the dayside high-density and dusk low-density regions predicted by the TGCM. The morphology of these density anomalies will be described in more detail in a later paper. The cause of the anomalies is not

clear at present and will be the subject of further investigation.

5. SUMMARY AND CONCLUSIONS

A degree of confidence in global thermospheric models has been established by their ability to predict seasonal and solar cycle variations. Numerical experiments also indicate that the TGCMs produce reasonable results for time-dependent simulations. Verification of the TGCMs by the simulation of many different events using realistic inputs and obtaining realistic outputs is now under way. The ETS interval of September 1984 provided an ideal opportunity to continue the verification process since large quantities of high-quality thermospheric data were obtained during an intensive coordinated campaign. This equinox solar minimum case also provides an interesting contrast to the equinox solar maximum simulations described by *Roble et al.* [1987].

Novel techniques were developed to specify the high-latitude convection and precipitation inputs for the TGCM, and to tune them for the ETS interval. The high-latitude convection patterns for the ETS interval were derived from the AMIE technique of *Richmond and Kamide* [1988], which provides a best fit potential pattern (in the least squares sense) to a variety of ionospheric data. Particle energies and the location and size of the auroral oval were tuned by reference to satellite data collected during the ETS period. Semidiurnal tides propagating from the lower atmosphere were also included in the present simulation.

The effects of both tides and high-latitude forcing on the quiet day global thermospheric morphology were described. The storm time response of the thermosphere was then contrasted with the quiet day, emphasizing the increased importance of high-latitude forcing. The enhanced auroral particle precipitation and magnetospheric convection during the magnetic storm led to large disturbances in the global circulation, temperature, and composition patterns. These disturbances propagated preferentially from high latitudes into the morning sector, which corresponded with the American sector in this case.

The penetration of storm effects from high to lower latitudes is very asymmetrical in the present study. In the American sector the $O/(O_2 + N_2)$ ratio was diminished as far equatorward as 30°N, while in other sectors, such as Europe, the decrease was limited to within 15° of the auroral oval. The penetration of storm effects into the American sector is largely due to the location of intense Joule heating in the early part of the storm. Presumably, the effects of the storm would have been modified if the Joule heating had been located in a different sector. In contrast with these results, *Rishbeth et al.* [1985] performed a numerical experiment using the UCL TGCM to investigate the compositional effects of a magnetic storm, and they obtained an increase in the mean molecular weight (equivalent to reduction of $O/O_2 + N_2$ ratio) only within a few degrees of the auroral oval in all longitude sectors. The apparent discrepancy in the latitudinal extent of compositional effects between the UCL TGCM and NCAR TGCM may possibly be due to the idealized high-latitude inputs used by Rishbeth et al. The present study reveals the sensitivity of the thermospheric response to details of the high-latitude forcing and indicates that simplified convection and auroral inputs may yield unrealistic effects. The composition changes predicted by the NCAR TGCM should have a profound effect on *F* region electron concentrations, particularly in the American sector, and will form the basis of a future study.

Previous work on composition changes during magnetic storms has emphasized the importance of vertical diffusion in maintaining diffusive equilibrium [e.g., *Rishbeth et al.*, 1985]. Poststorm recovery of thermospheric composition has also implicitly been assumed to be diffusion-driven. Unfortunately, the present TGCM simulation never recovered, in spite of running for a further 3 days with moderate high-latitude inputs. *Burns et al.* [this issue] describe how vertical advection appears to be the mechanism causing poststorm composition recovery, and how the inclusion of a self-consistent aeronomic scheme in the TGCM is necessary to achieve such a recovery.

A new and interesting feature of the polar cap thermosphere has been discovered in this simulation. A four-cell pattern of high and low densities is predicted for altitudes around 200 km following the storm. The exact location of the cells varies with universal time, but the high densities are generally displaced toward the noon and midnight sectors of the polar cap while the low densities are displaced in the dawn-dusk direction. The intensity of the density perturbations varies with magnetic activity. The detailed morphology of the four-cell density feature and satellite data supporting its existence will be discussed along with possible generation mechanisms in a forthcoming paper.

The objective of the ETS is to understand the thermospheric response to variable high-latitude forcing. *Crowley et al.* [this issue] will quantitatively assess the validity of this state of the art simulation. The model accurately reproduces many features of the ETS data and may therefore be considered realistic. Analysis of the model permits investigation of the observed phenomena and leads to an improved understanding of the thermosphere. Discrepancies between the predictions and observations yield additional insights, and suggestions will be made for improvements in future simulations.

Acknowledgments. This research effort was supported in part by the NASA Solar-Terrestrial Theory Program (NASA contract W-16, 320) and the Air Force Office of Scientific Research task 2310G9 (with the Air Force Geophysics Laboratory). We are grateful to Cassandra Fesen for helpful discussions concerning thermospheric tides.

The Editor thanks H. G. Mayr and R. W. Smith for their assistance in evaluating this paper.

REFERENCES

Bilitza, D., International reference ionosphere: Recent developments, *Radio Sci.*, *21*, 343–346, 1986.

Burns, A. G., T. L. Killeen, G. Crowley, B. A. Emery, and R. G. Roble, On the mechanisms responsible for high-latitude thermospheric composition variations during the recovery phase of a geomagnetic storm, *J. Geophys. Res.*, this issue.

Burnside, R. G., C. A. Tepley, and V. B. Wickwar, the O^+-O collision cross-section: Can it be inferred from aeronomical measurements?, *Ann. Geophys.*, *5*, 343–350, 1987.

Carlson, H. C., Jr., and G. Crowley, The Equinox Transition Study: An overview, *J. Geophys. Res.*, this issue.

Crowley, G., B. A. Emery, R. G. Roble, H. C. Carlson, Jr., J. E. Salah, V. B. Wickwar, K. L. Miller, W. L. Oliver, R. G. Burnside, and F. A. Marcos, Thermospheric dynamics during September 18–19, 1984, 2, Validation of the NCAR thermospheric general circulation model, *J. Geophys. Res.*, this issue.

Dickinson, R. E., E. C. Ridley, and R. G. Roble, A three-dimensional, time-dependent general circulation model of the thermosphere, *J. Geophys. Res.*, *86*, 1499–1512, 1981.

Dickinson, R. E., E. C. Ridley, and R. G. Roble, Thermospheric general circulation with coupled dynamics and composition, *J. Atmos. Sci.*, *41*, 205–219, 1984.

Emery, B. A., R. G. Roble, E. C. Ridley, D. J. Knipp, and G. Crowley, Parameterization of the ion convection and the auroral oval in the NCAR thermospheric general circulation model, technical report, High Altitude Obs., Boulder, Colo., 1989.

Fesen, C. G., R. E. Dickinson, and R. G. Roble, Simulation of thermospheric tides at equinox with the NCAR thermospheric general circulation model, *J. Geophys. Res.*, *91*, 4471–4489, 1986.

Fuller-Rowell, T. J., and D. S. Evans, Height-integrated Pedersen and Hall conductivity patterns inferred from the TIROS-NOAA satellite data, *J. Geophys. Res.*, *92*, 7606–7618, 1987.

Fuller-Rowell, T. J., and D. Rees, A three-dimensional, time-dependent global model of the thermosphere, *J. Atmos. Sci.*, *37*, 2545–2657, 1980.

Fuller-Rowell, T. J., and D. Rees, A three-dimensional, time-dependent simulation of the global dynamical response of the thermosphere to a geomagnetic substorm, *J. Atmos. Terr. Phys.*, *43*, 701–721, 1981.

Fuller-Rowell, T. J., and D. Rees, Derivation of a conservation equation for mean molecular weight for a two-constituent gas within a three-dimensional, time-dependent model of the thermosphere, *Planet. Space Sci.*, *31*, 1209–1222, 1983.

Fuller-Rowell, T. J., and D. Rees, Interpretation of an anticipated long-lived vortex in the lower thermosphere following simulation of an isolated substorm, *Planet. Space Sci.*, *32*, 69–85, 1984.

Fuller-Rowell, T. J., D. Rees, S. Quegan, G. J. Bailey, and R. J. Moffett, The effect of realistic conductivities on the high-latitude neutral thermospheric circulation, *Planet. Space Sci.*, *32*, 469–480, 1984.

Hays, P. B., et al., Observations of the dynamics of the polar thermosphere, *J. Geophys. Res.*, *89*, 5597–5612, 1984.

Heelis, R. A., J. K. Lowell, and R. W. Spiro, A model of the high-latitude ionospheric convection pattern, *J. Geophys. Res.*, *87*, 6339–6345, 1982.

Hernandez, G., and R. G. Roble, The geomagnetic quiet nighttime thermospheric wind pattern over Fritz Peak Observatory during solar cycle minimum and maximum, *J. Geophys. Res.*, *89*, 327–337, 1984*a*.

Hernandez, G., and R. G. Roble, Nighttime variation of thermospheric winds and temperatures over Fritz Peak Observatory during the geomagnetic storm of March 2, 1983, *J. Geophys. Res.*, *89*, 9049–9056, 1984*b*.

Herrero, F. A., H. G. Mayr, N. W. Spencer, A. E. Hedin, and B. G. Fejer, Interaction of zonal winds with the equatorial midnight pressure bulge in the Earth's thermosphere: Empirical check of momentum balance, *Geophys. Res. Lett.*, *12*, 491–494, 1985.

Killeen, T. L., and R. G. Roble, An analysis of the high-latitude thermospheric wind pattern calculated by a thermospheric general circulation model, 1, Momentum forcing, *J. Geophys. Res.*, *89*, 7509–7522, 1984.

Killeen, T. L., and R. G. Roble, An analysis of the high-latitude thermospheric wind pattern calculated by a thermospheric general circulation model, 2, Neutral parcel transport, *J. Geophys. Res.*, *91*, 11,291–11,307, 1986.

Knipp, D. J., et al., Electrodynamic patterns for September 19, 1984, *J. Geophys. Res.*, this issue.

Mayr, H. G., and H. Volland, Magnetic storm characteristics of the thermosphere, *J. Geophys. Res.*, *78*, 2251–2264, 1973.

Mayr, H. G., I. Harris, F. Varosi, and F. A. Herrero, Global excitation of wave phenomena in a dissipative multiconstituent medium, 1, Transfer function of the Earth's thermosphere, *J. Geophys. Res.*, *89*, 10,929–10,959, 1984*a*.

Mayr, H. G., I. Harris, F. Varosi, and F. A. Herrero, Global excitation of wave phenomena in a dissipative multiconstituent medium, 2, Impulsive perturbations in the Earth's thermosphere, *J. Geophys. Res.*, *89*, 10,961–10,986, 1984*b*.

Meriwether, J. W., Jr., P. Shih, T. L. Killeen, V. B. Wickwar, and R. G. Roble, Nighttime thermospheric winds over Sondre Stromfjord, Greenland, *Geophys. Res. Lett.*, *11*, 931–934, 1984.

Rees, D., The response of the high-latitude thermosphere to geomagnetic activity, *Adv. Space Res.*, *5*, 267–282, 1985.

Rees, D., T. J. Fuller-Rowell, and R. W. Smith, Measurements of high latitude thermospheric winds by rocket and ground-based techniques and their interpretation using a three-dimensional time-dependent dynamical model, *Planet. Space Sci.*, *28*, 919–932, 1980.

Rees, D., T. J. Fuller-Rowell, R. Gordon, T. L. Killeen, P. B. Hays, L. E. Wharton, and N. W. Spencer, A comparison of wind observations of the upper thermosphere from the Dynamics Explorer satellite with the predictions of a global time-dependent model, *Planet. Space Sci.*, *31*, 1299–1314, 1983.

Rees, D., M. F. Smith, and R. Gordon, The generation of vertical thermospheric winds and gravity waves at auroral latitudes, II, Theory and numerical modeling of vertical winds, *Planet. Space Sci.*, *32*, 685–705, 1984.

Rees, D., T. J. Fuller-Rowell, M. F. Smith, R. Gordon, T. L. Killeen, P. B. Hays, N. W. Spencer, L. E. Wharton, and N. C. Maynard, The westward thermospheric jet-stream of the evening auroral oval, *Planet. Space Sci.*, *33*, 425–456, 1985.

Rees, D., T. J. Fuller-Rowell, R. Gordon, J. P. Heppner, N. C. Maynard, N. W. Spencer, L. E. Wharton, P. B. Hays, and T. L. Killeen, A theoretical and empirical study of the response of the high-latitude thermosphere to the sense of the "*Y*" component of the interplanetary magnetic field, *Planet. Space Sci.*, *34*, 1–40, 1986.

Richmond, A. D., and Y. Kamide, Mapping electrodynamic features of the high-latitude ionosphere from localized observations: Technique, *J. Geophys. Res.*, *93*, 5741–5759, 1988.

Richmond, A. D., et al., Mapping electrodynamic features of the high-latitude ionosphere from localized observations: Combined incoherent-scatter radar and magnetometer measurements for 1984 January 18–19, *J. Geophys. Res.*, *93*, 5760–5776, 1988.

Rishbeth, H., and O. K. Garriott, *Introduction to Ionospheric Physics*, chap. 8, Academic, San Diego, Calif., 1969.

Rishbeth, H., R. Gordon, D. Rees, and T. J. Fuller-Rowell, Modelling of thermospheric composition changes caused by a severe magnetic storm, *Planet. Space Sci.*, *33*, 1283–1301, 1985.

Roble, R. G., and E. C. Ridley, An auroral model for the NCAR thermospheric general circulation model (TGCM), *Ann. Geophys., Ser. A*, *5*(6), 369–382, 1987.

Roble, R. G., R. E. Dickinson, and E. C. Ridley, Seasonal and solar cycle variations of the zonal mean circulation in the thermosphere, *J. Geophys. Res.*, *82*, 5493–5504, 1977.

Roble, R. G., R. E. Dickinson, and E. C. Ridley, Global circulation and temperature structure of the thermosphere with high-latitude plasma convection, *J. Geophys. Res.*, *87*, 1599–1614, 1982.

Roble, R. G., R. E. Dickinson, E. C. Ridley, B. A. Emery, P. B. Hays, T. L. Killeen, and N. W. Spencer, The high latitude circulation and temperature structure of the thermosphere near solstice, *Planet. Space Sci.*, *31*, 1479–1499, 1983.

Roble, R. G., B. A. Emery, R. E. Dickinson, E. C. Ridley, T. L. Killeen, P. B. Hays, G. R. Carignan, and N. W. Spencer, Thermospheric circulation, temperature, and compositional structure of the southern hemisphere polar cap during October–November 1981, *J. Geophys. Res.*, *89*, 9057–9068, 1984.

Roble, R. G., J. M. Forbes, and F. A. Marcos, Thermospheric dynamics during the March 22, 1979, magnetic storm, 1, Model simulations, *J. Geophys. Res.*, *92*, 6045–6068, 1987.

Roble, R. G., T. L. Killeen, N. W. Spencer, R. A. Heelis, P. H. Reiff, and J. D. Winningham, Thermospheric dynamics during November 21–22, 1981: Dynamics Explorer measurements and thermospheric general circulation model predictions, *J. Geophys. Res.*, *93*, 209–245, 1988.

Schunk, R. W., and J. C. G. Walker, Theoretical ion densities in the lower ionosphere, *Planet. Space Sci.*, *21*, 1875–1896, 1973.

Sica, R. J., M. H. Rees, G. J. Romick, G. Hernandez, and R. G. Roble, Auroral zone thermospheric dynamics, 1, Averages, *J. Geophys. Res.*, *91*, 3231–3244, 1986*a*.

Sica, R. J., G. Hernandez, G. J. Romick, M. H. Rees, and R. G. Roble, Auroral zone thermospheric dynamics, 2, Individual nights, *J. Geophys. Res.*, *91*, 13,593–13,611, 1986*b*.

Sipler, D. P., M. A. Biondi, and R. G. Roble, Midlatitude *F*-region neutral winds and temperatures during the priority regular world day 14 August 1980, *Planet. Space Sci.*, *29*, 1367–1372, 1981.

Sipler, D. P., M. A. Biondi, and R. G. Roble, *F*-region neutral winds and temperatures at equatorial latitudes: Measured and predicted

behavior during geomagnetically quiet conditions, *Planet. Space Sci., 31*, 53–66, 1983.

Smith, M. F., D. Rees, and T. J. Fuller-Rowell, The consequences of high latitude particle precipitation on global thermospheric dynamics, *Planet. Space Sci., 30*, 1259–1267, 1982.

Spencer, N. W., G. R. Carignan, H. G. Mayr, H. B. Niemann, R. F. Theis, and L. E. Wharton, The midnight temperature maximum in the Earth's equatorial thermosphere, *Geophys. Res. Lett., 6*, 444–446, 1979.

Volland, H., A model of the magnetospheric electric convection field, *J. Geophys. Res., 83*, 2695–2699, 1978.

H. C. Carlson, Jr., Air Force Geophysics Laboratory, Hanscom Air Force Base, Bedford, MA 01731.

G. Crowley, Center for Atmospheric Research, University of Lowell, 450 Aiken Street, Lowell, MA 01854.

B. A. Emery and R. G. Roble, High Altitude Observatory, National Center for Atmospheric Research, P.O. Box 3000, Boulder, CO 80307.

D. J. Knipp, Physics Department, U.S. Air Force Academy, Colorado Springs, CO 80840.

(Received March 13, 1989;
revised July 17, 1989;
accepted July 18, 1989.)